PhD in

INNOVATIVE TECHNOLOGIES IN DISEASES OF SKELETON, SKIN AND ORAL-CRANIOFACIAL DISTRICT

XXXIV cycle

Anti-neoplastic effects of novel compounds on human head & neck squamous carcinoma cell lines

Supervisor

Prof. Marco Artico

Candidate

Alice Nicolai

Academic Year 2020-2021

INDEX

1.Introduction

1.1 HNSCC, head and neck squamous cell carcinoma

1.1.1 HNSCC: generalities

Human head and neck squamous cell carcinomas (HNSCC) are a group of tumors that, developing in the mucosal linings of the superior aerodigestive tract, can affect various regions of the oral cavity, oropharynx, hypopharynx and larynx [1][2]. Oral cavity cancers represent 25% of all head and neck carcinomas [3]. This type of neoplasm is extremely aggressive and is the sixth leading cause of cancer worldwide with 890,000 new cases and 450,000 deaths in 2018 [2][4]. More than half a million new cases are diagnosed per year and almost 50% of patients have a less than 5 years survival rate [1].

The HNSCC incidence is constantly growing and is foretold to rise by around 30%, which means 1.08 million new cases per year, by 2030 [4].

Men are predisposed to develop HNSCC, 2-4 more than women [5][6]. Most of these tumors are correlated to human papillomavirus (HPV) infection and the incidence of HPV-related HNSCC increased in the last years. The average age for oropharyngeal cancer associated with HPV diagnosis is about 53 years while for not- virally associated cancer is 66 years [4].

Besides deaths directly attributable to cancer, it is detected a high-level of suicides among survivors due to compromised quality of life and psychological problems [4]. HNSCC have the second-highest rate of survivor suicides (63.4 cases per 100,000 people) after pancreatic cancer. It is a very high number when compared with other cancers (23.6 cases per 100,000 people) [7].

1.1.2 Risk factors in HNSCC

The main risk factors for HNSCC development, by relying on epidemiological studies, are environmental pollution, tobacco and alcohol abuse and viral infection (Fig. 1) [4]. As regards infectious agents, chronic Human Papilloma Virus (HPV) and Epstein-Barr Virus

(EBV) infections are known risk factors for oropharyngeal and nasopharyngeal carcinomas, respectively [8][9].

Oral cavity and larynx cancers are mostly related to tobacco smoking and alcohol abuse, while pharynx tumors to high-risk HPV infection, mainly HPV-16 [4][2]. Furthermore, both ones can be caused also by genetic predisposition [2]. An example is represented by patients suffering from Fanconi anaemia, a rare genetic disease marked by compromised DNA repair. These patients have a 500–700-fold increased risk to develop HNSCC [10][4].

Besides, some Asia-Pacific populations develop oral cavity cancer probably related to areca nut products chewing such as "*betel quid*": a variety of personalised combinations including areca, betel leaf (the leaf of Piper betel), slaked lime and tobacco [4].

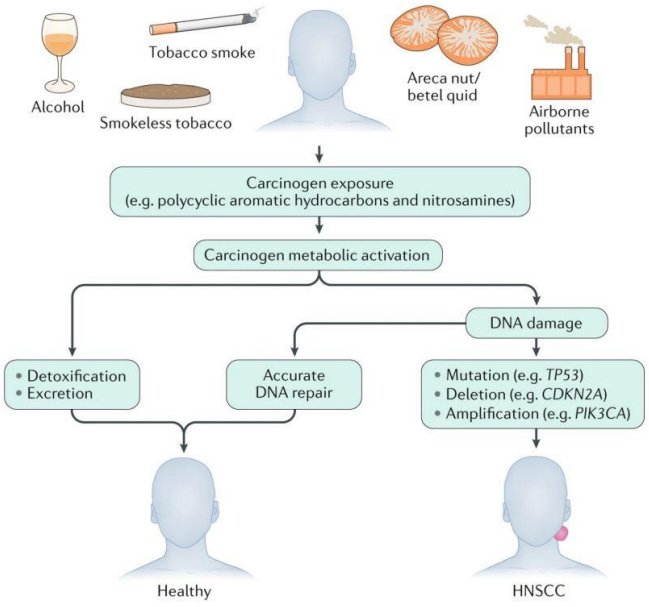

Figure 1: Main risk factors in HNSCC [4].

To sum up, the overall incidence of HNSCC should be cut down by reducing tobacco consumption, improving oral health and spreading HPV vaccination [11].

1.1.3 HNSCC pathogenesis and treatments

The oral cavity, pharynx, larynx and sinonasal tract are coated by mucosal epithelial cells. Histologically, HNSCC cancer derives from this coating, however, the cell that gives origin to the lesion depends on two factors:

- Anatomical site.
- Causative agent.

Though, the main candidates are the adult stem cells or progenitor cells because of their capacity to give rise to cancer stem cells (CSCs) with self-renewal and pluripotency properties.
The passages leading to the invasive phenotype are represented by hyperplasia of epithelial cells, dysplasia, carcinoma *in situ* and invasive carcinoma (Fig. 2) [4].

Figure 2: Representation of HNSCC progression [4]. (Modified by this article).

Tobacco, with over 5000 chemicals, many of which are potentially carcinogenic, is the main cause of HPV-negative HNSCC development [4].

The most important carcinogenic effects of tobacco chemicals are caused by polycyclic aromatic hydrocarbons (PAHs) [12][13]. In areca nut and betel quid carcinogens are not well-defined, while in smoke-free tobacco the main carcinogen are nitrosamines [14][4].

Carcinogenic substances of tobacco, including PAHs and nitrosamines, as well as acting as carcinogenic triggers by themselves, may, because of their metabolic activation, generate reactive metabolites that can covalently bind to DNA. All this can lead to the further development of mutations and other genetic abnormalities [4].

In addition, the tobacco-related carcinogenicity has been associated with the inflammation process in tobacco carcinogen exposed tissues which can contribute to malignant progression with production of cytokines, chemokines and growth factors [15].

As regard alcohol abuse, two probable carcinogenic activities are leading to HPV-negative HNSCC [15]:

- Being a solvent for other carcinogenic substances improving tissue exposure [16].
- Being metabolized to acetaldehyde, an active substance rarely forming adducts with DNA [17].

Finally, 70% of oropharyngeal tumors are associated with HPV infection. Most of these HPV-HNSCC come from deep crypts in the palatine and lingual tonsils. Among various types of HPVs, the main responsible is HPV-16, but also other etiological agents can be identified in different high-risk HPV including HPV-18, HPV-31, HPV-33 and HPV-52 [4].

The main locally confined HNSCC treatments are surgical resection and radiotherapy. The aim is to achieve the highest level of healing while preserving oral function. Currently, the treatment engages surgery and consequent chemoradiotherapy (CRT) for oral cavity cancers and primary CRT for pharynx and larynx ones [4].

Patients affected by HNSCC with no lymph node involvement and metastasis or with single node involvement, are treated by one intervention, such as resection or radiation, which results in over 80% cure rate [18].

For more advanced stadium or nodal involvement cancers, post-operative radiotherapy or chemoradiotherapy cut down the risk of relapse and increase survival rate [19][20].

Recurrent or metastatic HNSCC are normally treated with surgical resection, re-irradiation or metastases surgical removal [21][22]. Other patients, except those who for previous autoimmune diseases are contraindicated for this approach, receive the first-line systemic therapy with pembrolizumab, an immune checkpoint inhibitor.
This compound is a humanized IgG4 antibody against programmed cell death protein 1 (PD-1) which is generally used in patients whose carcinoma is characterized by the expression of PD-L1 (one of the two PD-1 ligands) or microsatellite instability [4].

PD-1 is an immune checkpoint that can avoid the tumor cell damaged by the immune system and autoimmune disorder beginning [23]. When compared pembrolizumab and cetuximab chemotherapy resulting data showed comparable toxicity and therapeutic response but, pembrolizumab therapy improved the overall patient survival (10.7 months with cetuximab to 13 months with pembrolizumab) [4].

Patients who cannot be treated with first-line immunotherapy are treated with cetuximab and combined chemotherapy consisting of a platinating agent with 5-fluorouracil or paclitaxel [24].

However, despite some patients had a history of autoimmune disease, in case of poor prognosis, PD-1 can be revaluated as a target in their cancer therapy [4].

For metastatic and chronic diseases, recent immunotherapies are currently being tested, in addition to hopeful combinations based on immune checkpoint inhibition with kinase inhibitors or anti-angiogenic compounds [25].

1.1.4 Tumor microenvironment and metastasis

The HNSCC tumor microenvironment is characterized by a heterogeneous mix based on various cancer and stromal cells such as cancer-associated fibroblasts (CAFs), immune and endothelial cells, [4] but also peripheral nervous system innervating neurons and adrenergic neurons inducing cancer growth [26].

Cancer-associated fibroblasts produce different molecules involved in tumor growth since they support angiogenesis, immunosuppressive cell enrolment, as well as extracellular matrix (ECM) degradation and remodelling [4].

These products include growth factors, like EGF, VEGF and HGF, cytokines like IL-6, chemokines and matrix metalloproteases (MMPs) [27][28].

The oral microbiome composition is also interesting since in oral cancer the possible role of highly specific bacterial and fungal agents has been highlighted and still examined [29][30].

Head and neck squamous cell carcinomas can feature a high level of hypoxia [31] and this suggests poor prognosis and cancer survival after radiation therapy [32][33].

As regard the genetic field, hypoxia in cancer cells determines the expression of hypoxia-inducible factor (HIF1α), a transcription factor HIF1 subunit.

HIF1α directs the expression of genes encoding MMPs and vascular endothelial growth factor (VEGF), which promote tumor cell infiltration and angiogenesis, respectively [4].

It has been shown that the majority of HNSCC cancers present an extremely immunosuppressive tumor microenvironment [34][35].

TME is characterized by T_{eff} cells, NK cells, T_{reg} cells, derived suppression cells (MDSCs) and M2 macrophages. The first two drive anti-cancer immunity, while the remnants immune system suppression and cancer cell proliferation [4].

Numerous immune cells infiltrate HNSCC and their composition depends on:

- Anatomical localization.
- Cancer-causing agent, such as tobacco consumption and viral agent [34][36].

The invasive and metastatic process of HNSCC cells follows different pathways. Both cancer and stromal cells produce metalloproteases that promote cell invasion since their involvement in extra-cellular matrix degradation and reshaping. In addition, a relationship has been found between high levels of some metalloproteases (MMP1, MMP2, MMP9 and MMP13) and a high invasive carcinoma with a tendency to metastasize and a resulting poor prognosis [37][38].

The epithelial-mesenchymal transition (EMT) has particular importance in metastasis formation. During EMT cells down-regulate E-cadherin, while up-regulate N-cadherin and vimentin, resulting in a cell adhesion decrement, an improved migration activity and invasive ability. Indeed, a relation has been detected between variations in cadherin and vimentin concentrations and increased metastasis formation in HNSCC [28][39].

In addition, high levels of hypoxia can be linked with metastasis [32][40][41]. This depends on HIF α, whose expression is caused by high levels of hypoxia, which lead to the expression of vimentin, TWIST and SNAIL (which mediate down-regulation of E-cadherin during EMT) [28]. We can conclude that hypoxic conditions may drive cancer cells to transition from an epithelial to a mesenchymal phenotype [4].

Two other important correlations were highlighted:

- EMT and stem cell property asset such as HNSCC CSC markers expression [42].
- CD44, CD133 or ALDH1 expression by HNSCC cells and metastasis [43].

1.1.5 Deregulated pathways and genomic alterations in HNSCC

HNSCC outgrowth is mainly related to deregulated pathways and genetic or epigenetic abnormalities. Indeed, these carcinomas are characterized by repeated loss or gain of chromosomal loci [44].

Different chromosomal alterations take place in different cancer progression phases, it's believed that several genetic abnormalities are needed for the complete turning into invasive HNSCC (Fig. 2) [16][4].

The alterations mainly associated with HPV-negative tumor could be summed as follow:

- The passage from normal cells to hyperplasia involves the region 9p21 loss (9p21 locus contains tumor suppressor genes).
- Advancement from hyperplasia to dysplasia is characterized by loss of 17p13 and 3p21.
- During dysplasia to carcinoma in *situ* progression appears 11q13, 14q32 and 13q21 loss.
- In the end loss of 10q23, 4q27, 6p and 8 evident during the final step to invasive carcinoma. [4]

HNSCC pathogenesis is often driven by tumor suppressor loss rather than by oncogene activation, contrary to various malignant solid cancers: the only oncogene appearing to be commonly altered in HNSCC (~14%) is PIK3CA, which encodes the catalytic subunit of 3-kinase phosphoinositide (PI3K) [44][45][46], while mutations in RAS genes are rare, about 4% of HNSCC. NRF2 and KEAP1 encoding genes are crucial regulators in oxidative stress conditions and are often subject to mutation entirely in HNSCC HPV-negative [44].

Oncogenic pathways involve also epigenetic changes; CDKN2A, RARB (encoding Rarβ, a mediator in the epithelial cells differentiation), DCC and MGMT (a protein involved in repairing DNA damage caused by tobacco carcinogens) are key cancer suppressors often hypermethylated and under-regulated in HNSCC [47][48].

Several studies detected in HNSCC tumors unusual activation of signalling pathways and several abnormal expressions of proteins involved in that signals, including:

- Cytokine IL-6 and its receptor overexpression [49][50]
- Cyclin D1 overexpression that is related to poor clinical survival [16][51].

In the end, EGFR overexpression is detected in 80-90% of head and neck squamous cell carcinomas. That's the reason why it could be considered a prognostic marker since its expression is related to poor prognosis and progression-free survival [52][53].

Several signalling pathways are leading to tumor growth, the most common of which is the alteration of the PI3K-AKT-mTOR pathway [44][54].

WNT-β-catenin oncogenic pathway provides to HNSCC oncogenesis too [55], as well as the RAS-MAPK signalling, that is involved in more prospering cell growth and survival [44].

Last, also STAT3 signalling is involved, since it induces the expression of diverse genes such as genes encoding VEGF, IL-6, IL-10 and TGFβ (promoters of cell growth and immunosuppressive condition) [56].

1.2 Anti-mitotic agents

Anti-mitotic agents lead to cell cycle arrest in the G2/M phase and induce the apoptotic cell death with consequent tumor regression. For this reason, these compounds are commonly employed as anti-neoplastic drugs [57]. Anti-tubulin agents and kinesin inhibitors are two important members of this class of drugs and are going to be analysed below.

1.2.1 Anti-tubulin agents

Anti-tubulin agents are anti-cancer drugs that, interfering with tubulin and microtubule dynamics, lead to a proliferation arrest by triggering a *suicide* effect (apoptosis cell death). The role of the cytoskeleton in cell division, indeed, makes them a common target in anti-neoplastic therapy [58][59][60].

However, it's important to stress a limited clinical use of diverse tubulin inhibitors in anti-cancer therapy caused by neurotoxicity development as a side effect and the multidrug resistance mechanisms (based on drug efflux pumps and βIII tubulin isoform expression) [61]. It means new inhibitors, acting differently but still by binding to tubulin, are required [57].

The anti-microtubular drug effect in anti-tumor therapy can be boosted by using agents that have anti-apoptotic proteins as target, since one mechanism used by cells to overcome anti-microtubular effects is to hang on apoptotic process [62]. It's needed to mention taxanes and vinca alkaloids that have been used in clinical studies for decades [62].

Taxanes target intracellular free tubulin and lead to stable microtubule assembly. Paclitaxel, docetaxel and cabazitaxel are taxanes approved by the FDA [63]. Paclitaxel was discovered in 1960. It is the only natural taxoid in this class of drugs and is extracted from the *taxus brevifolia* cortex, a North American pacific yew tree [64]. Its use is limited by bark extraction and new compounds have been synthesized: Docetaxel e Cabazitaxel, semisynthetic taxoids derived from 10-deacetylbaccatin III, an unused compound since its inactivity [63]. The advantage of 10-deacetylbaccatin III is its extraction from leaves of the European yew tree *Taxus Baccata* which means that the tree, contrary to the cortex extraction, does not need to be cut and the extractable quantities can be more since leaves are a renewable source [63]. However, the taxane application is limited by numerous side effects including peripheral neuropathy, hypersensitivity reactions and haematological toxicity. On the other hand, a large proportion of taxanes-treated patients do not benefit from this treatment. This is probably due to a tumor insensitivity or a failure to reach adequate concentration at the site of action [63].

Vinca alkaloids will be analysed below.

1.2.1.1 Tubulin and microtubules

Tubulin is an intracellular protein: α and β tubulin monomers can exist as diverse isotypes characterized by distinct sequences of amino acids. These ones are obviously encoded by different genes [62]. Tubulin intracellular concentration is about 5 μM, not depending on the cell cycle phase. Its concentration, in truth, changes according to cell type but, basically, constitutes on average the 4.5-5% of total soluble cell proteins [65][66].

Determined tubulin isotypes have been associated with neoplastic cells and can have prognostic value in solid cancers. An example is the overexpression of βIII-tubulin that has been recognized as a potential marker for aggressive phenotypes in different cancer diseases [67].

It has also been shown that the life expectancy of patients whose cancer overexpress βII-tubulin isotype is short, especially if it has nuclear localization. Indeed, the βII subunit enhances tumor cell growth and invasion, for this reason, its appearance and cellular localization can be considered potential prognostic markers [62]. Tubulin mutations and its various isotypes in invasive cancers can play a role in drug resistance because of their impact on the anti-neoplastic compound binding site [62].

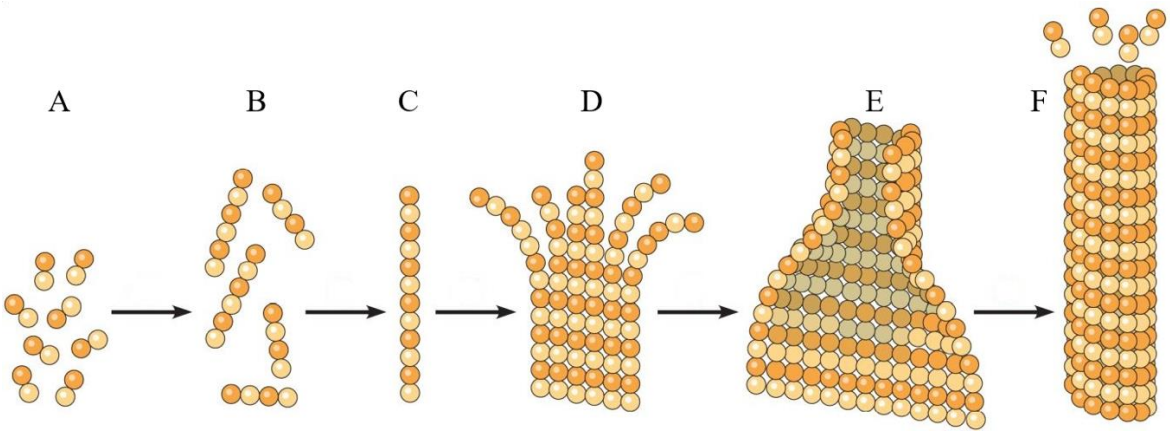

Figure 3: Microtubule assembly. A: Dimers of tubulin; B: Oligomers of tubulin; C: Protofilaments; D: Turn of protofilament; E: Closing microtubule; F: Stretching microtubule.

Microtubules are tubular polymers of tubulin and are the cytoskeleton base elements in eukaryotic cells. Their organization consists of 13 assembled protofilaments with head-tail alignment made of αβ-tubulin heterodimers arranged to form cylinders of 25 nm diameter [68].

Microtubules take part in several vital cell functions: chromosome segregation during cell division, cellular vesicle transportation, organelle delivery and cell invasion [69]. The tubular structure awards microtubules an intrinsic polarity [70][71]; the two extremities have a different cellular localization: the one presenting α-tubulin is in the *centrosome*, the central part of the cell, while the β-tubulin end is in the cell periphery. This extreme, also known as `+´ end, being very dynamic, is subject to continuous polymerization-depolymerization phases [71].

The cytoskeleton is a network with a radial arrangement that is organized in a central structure near the nucleus, the *centrosome*. Its organization is subject to changes during cell division, first depolymerises and then the single tubulin components reassemble (repolarization) to form a mitotic spindle [68].

Several cell factors are involved in the regulation of microtubule polymerization-depolymerization but the main implicated are microtubule-associated proteins (MAPs) [58].

1.2.1.2 Anti-tubulin depolymerization agents

It's useful to subdivide tubulin inhibitors into two groups: microtubule-stabilizing agents, such as taxanes, epothilones, laulimalide and destabilizing agents including vinca alkaloids and colchicine binding site agents (Fig. 4) [61].

Epothilones have an anti-cancer taxol-like mechanism and laulimalide at high concentrations stabilises microtubule organization and prevents cell division in a comparable way to paclitaxel but their binding sites on microtubule are distinct [72][73].

Tubulin inhibitors used as anti-neoplastic drugs target the taxane or vinca alkaloid binding site, however many of these compounds are characterised by drug resistance [61].

While colchicine cannot be utilized in cancer therapy because of its toxicity, other inhibitors that bind to colchicine binding site in the α-β-tubulin edge, are currently being studied as anti-tumor compounds since diverse studies have previously detected that colchicine binding agents can get over drug resistance mediated by P-glycoprotein overexpression and βIII tubulin isoforms [61].

Figure 4: Representation of some anti-microtubule agents binding site.

Vinca alkaloids consist of diverse compounds: one of these, vinblastine was isolated in 1958 and the others, vincristine, vinorelbine, vindesine, vinpocetine have been later synthesized [74].

Vinflunine is a new semi-synthetic vinca alkaloid that is presently being examined in clinical trials showing a higher anti-neoplastic action than the other vinca alkaloids and less neurotoxicity in comparison to vinorelbine [74][75].

Vinca alkaloids are anti-cancer drugs that inhibit cell division and lead to mitosis arrest by binding to intracellular tubulin. They also act by reducing purine and RNA synthesis thanks to their contribution to dividing cells death. Although their action, vinca alkaloids reveal a limited application in clinical trials due to their inclination to develop multidrug resistance and serious side effects [74].

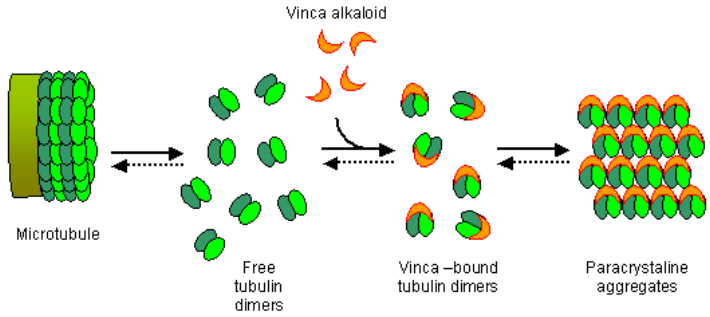

Figure 5: Simplify representation of vinca alkaloids action mechanism.

Vincristine is a natural vinca alkaloid that acts as an anti-cancer agent causing microtubule depolymerization. This alkaloid leads to metaphase arrest and apoptosis death during the mitosis process by binding to tubulin. For this reason, it has been used in tumor therapy since 1960 as an M-phase cell cycle-specific anti-neoplastic agent, but its clinical application is limited by neurotoxic side effects [74].

Vinblastine, just like vincristine, has been used as an anti-neoplastic drug, but it is characterised by toxic side effects. Vinblastine can avoid tubulin polymerization resulting in lower cancer growth and in restrained malignant angiogenesis too [74].

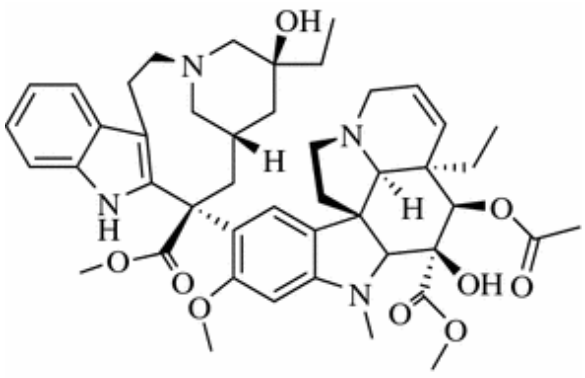

Figure 6: Vinblastine structure.

Vinorelbine is a semi-synthetic vinca alkaloid with more anti-cancer activity and less neurotoxicity than vincristine and vinblastine. This alkaloid is mostly utilized in advanced or metastatic non-small-cell lung cancer and advanced breast cancer [76][77].

In the end, Vindesine is a semisynthetic vinca alkaloid structurally correlated with vinblastine: deacetyl-vinblastine-amide. Indeed, its effects are comparable to those of vinblastine and it is utilised in therapy in various diseases such as malignant melanoma, chronic myeloid leukemia, acute lymphocytic leukemia, metastatic colorectal, breast cancer, pediatric solid tumors, renal and esophageal carcinomas [74][75][78].

Vinca alkaloids applications as anti-cancer drugs are restricted by their side effects; however, novel drug delivery systems and combination therapy could represent the right approaches for reducing their toxicity. Combination therapy consists of co-administration (simultaneously or sequentially) of vinca alkaloids with another chemotherapeutic to reach an increased anti-tumor effect [74][79].

On the other hand, also drug delivery systems are promising. For example, liposome-entrapped drugs improve the drug half-life and are not irritating at the tissue injection site [74].

1.2.1.3 Nocodazole

Nocodazole is a benzimidazol-2-yl carbamate ester derived molecule. Many studies indicated benzimidazole as the most well-known heterocycle because of its cytotoxic abilities and anti-tumor activity [80][81].

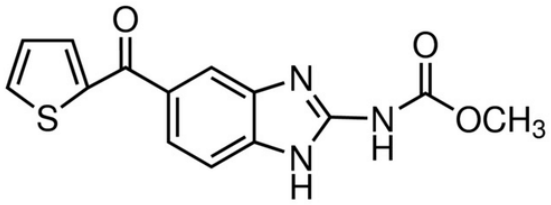

Figure 7: Nocodazole structure.

It targets beta-tubulin by developing hydrogen bonds among single beta subunits. Its interaction prevents the link between alpha and beta subunits [82][83]. This avoided tubulin heterodimer shaping lead to microtubule depolymerization. The final effect is an altered mitotic spindle assembly and the cell inability to perform mitosis [84][85].

Nocodazole is specific for high replication rate cells, as typical cancer cells. This compound determines a cell cycle block in G2 or M phase. A protracted stop in pro-metaphase is a probable starting point to apoptosis [86] and, since nocodazole is specific for replication cells, we can consider this molecule a promising anti-tumor compound.

Nocodazole has been shown to induce apoptosis in leukemic cells and at the same time does not interfere with the survival of T-lymphocytes and mesenchymal stromal cells in chronic lymphocytic leukemia [87]. But despite what said before, this compound has not yet come into the clinical studies [88].

1.2.2 Kinesin inhibitors

The cytoskeleton is composed by a network of microtubules and is involved in several cell activities, such as mitosis, cell movement and intracellular molecule transportation. Therefore, it is vital for central nervous system function, including axonal transport. Identifying and targeting microtubule-associated proteins (MAPs) is the aim of numerous studies because neurotoxicity is the dose-limiting side effect of many anti-microtubule agents [89]. The goal is to stop mitosis of tumor cells without generating neurotoxicity.

Among MAPs the mitotic kinesins stand out. This is a group of molecular motor proteins managing several steps during mitotic phase [90].

Currently, some mitotic kinesins inhibitors have been developed and used in both preclinical and clinical studies demonstrating to not produce neurotoxicity, as required [91].

1.2.2.1 Mitotic kinesin

The kinesins are numerous families of microtubule-based motor proteins and are important in cell survival [92]. Mitotic kinesins are a sub-group of kinesins. They act only during mitotic phase in cell division.

A kinesin can be divided into 3 main regions: a 340 amino acid motor domain (called “head” region), a “stalk” region and a “tail” region. The “head” region includes a microtubule-binding pocket and an ATP binding pocket (Fig. 8) [92].

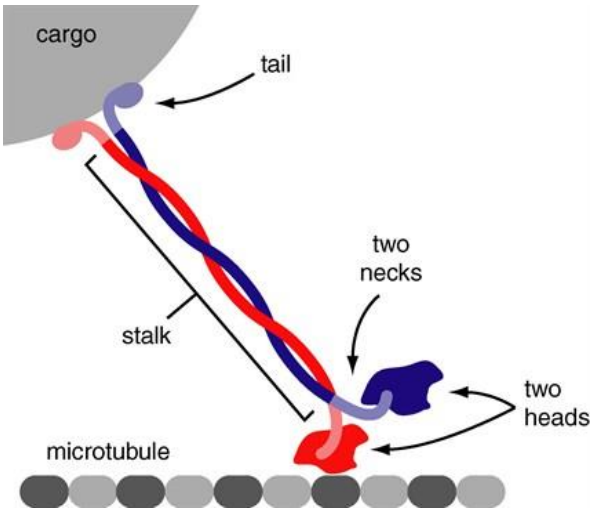

Figure 8: Kinesin structure.

Microtubules play an important role during chromosome alignment and segregation in eukaryotic cells by drawing tracks for vesicle and macromolecule active transportation and producing traction forces leading to mitotic spindle formation [93][94].

MTs are made up of repeating 8-nm-long tubulin polymers arranged in dimers that constitute the binding site (one in each dimer) for kinesin motor domain that moves along the microtubule. ATP hydrolysis is used by kinesin to produce force and movement along microtubules [95].

Microtubules are used as tracks by fourteen kinesin motor subfamilies. Kinesin-5 motors represent one of these subfamilies with a crucial function during metaphase, in mitotic spindle formation and during anaphase, in spindle elongation [94].

1.2.2.2 Kinesin spindle protein Eg5

Eg5 is a mitotic kinesin deemed as a promising target in cancer treatment because is overexpressed in several high-rate proliferation tumors while is almost not reported in non-proliferative tissues [96]. Eg5 inhibition leads to apoptosis death in many cancer cell lines

[97]: kinesin-5 motors stimulate microtubule crosslinking and elongation during mitotic spindle organization [94] and if mitotic spindle doesn't not assembly, chromosomal segregation doesn't take place and activation of checkpoint proteins lead to mitotic phase stop and cell division inhibition [96].

It's important to explain its organization: kinesin-5 motors, contrary to the other classes of kinesin, have a bipolar homo-tetrameric arrangement made up of about 320 amino acids, composed of two identical light chains and two identical heavy chains arranged in dimeric subunits set in an anti-parallel organization granted in the centre by a 60-nm-long-filament [94][98][99].

Kinesin-5 motor conserved organization involves an N-terminal motor domain that binds and hydrolyzes ATP, an α-helical coiled-coil stalk domain and a C-terminal tail domain [94].

The kinesin-5 preserved anti-parallel MTs moving activity is crucial in the mitotic spindle formation and extension. Indeed, this activity, due to the interaction between tail and motor domains at both ends of the kinesin-5 homo-tetramer allows kinesin-5 motors to activate at the same time all their MTs tracks as transport loads [94].

The kinesin-5 tail domain role is to link and stabilise the motor domain into its ADP (or nucleotide-free) arrangement to cut down ATP hydrolysis promoted by microtubules [94].

This is because, in either ADP MT-bound or the nucleotide-free state, the motor domain is bounded by the N-terminal subdomain of the tail domain. The kinesin-5 subdomain rotates from the MT- nucleotide-free network to the ATP-like state to bind the nucleotide. The final effect is a reduced ability of each active site in the motor domain to bind ATP during the ATP catalytic process [94].

1.2.2.3 Eg5 overexpression in laryngeal squamous cell carcinoma

In transformed cells, the Eg5 overexpression determines an additional force during the mitosis process promoting, excessively, the separation of sister chromatids and resulting in the possible monopolar spindle assembly. The main consequence is the formation of aneuploid daughter cells during the anaphase step. Furthermore, the acquisition or loss of

genetic material in aneuploid cells is deemed to play a crucial role in neoplastic formation [96].

Lu et al in 2016 was the first group to discover the Eg5 overexpression in laryngeal squamous cell carcinoma (LSCC), making this kinesin a hopeful new prognostic biomarker for LSCC patients [100].

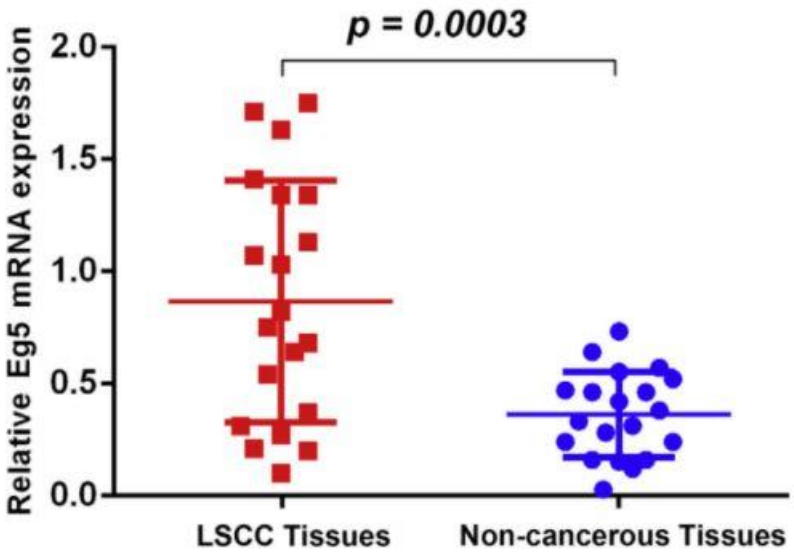

Figure 9: Eg5 mRNA expression levels in LSCC compared with non-cancerous tissues detect by qPCR [101].

The data of One-step quantitative polymerase chain reaction (qPCR) (Fig. 9) demonstrated that Eg5 mRNA expression levels in LSCC tissues are extraordinarily higher than in not-cancerous ones. That result was confirmed by ICH analyses showing that Eg5 protein expression in LSCC was statistically more than in other not-altered tissues [100].

Furthermore, previous studies revealed a significant relationship between high Eg5 expression and poor prognosis in renal, bladder, and prostate cancer [101][102][103].

The Eg5 overexpression can lead to forced microtubule change, bringing to spindle formation and compromised chromosomal segregation resulting, in the cellular level, in a disturbed spindle aggregation and mitotic slip [100]. These data suggest Eg5 as a smart target for anti-mitotic cancer agents.

1.2.2.4 Kinesin Eg5 inhibitors

Eg5 is involved in bipolar spindle assembly. The passage from one cell cycle phase to the next one is regulated by cell cycle checkpoints. If some defects occur in checkpoint activity, genetic mutations and chromosomal damage can be observed. Current studies proposed defected spindle checkpoints as making cells insensitive to anti-microtubule compounds. Therefore, new target therapy is required to block metaphase without modifying microtubule arrangement. Consequently, anti-mitotic agents targeting different elements involved in spindle formation could represent a new generation of anti-neoplastic drugs [97].

Mitotic kinesins, such as Eg5, are crucial regulators in the mitotic process; therefore, several kinesin Eg5 inhibitor compounds have been discovered: S-trityl-l-cystein, ispinesib, monastrol [97]. These inhibitors bind to an allosteric site among the helix 3 and loop 5 in the Eg5 domain. Only the kinesin-5 class show an extended loop 5, which means that Eg5 inhibitors have a high specificity [99].

Eg5 inhibition leads to form a monopolar spindle called “monoaster” surrounded by condensed chromosomes in a rosette-like arrangement. By avoiding centrosome separation and inducing the monopolar spindle formation, these inhibitors cause the activation of spindle checkpoint proteins leading to mitotic arrest without microtubule reorganization [97].

Many other Eg5 inhibitors have been discovered: they block the mitotic process and lead to cell death in proliferative tissues by a competitive ATP inhibition or binding another site in Eg5. These inhibitors do not show neuropathic side effects commonly identified in other anti-mitotic agents like taxol and vinca alkaloids. Eg5 inhibitors, also, reveal almost no effect on tubulin, thus they could be used to treat cancer that develops taxol resistance [99].

Some of these inhibitors are utilized in phase I or phase II clinical trials as anti-tumor compounds [99]. Results have shown that almost all tested inhibitors are well tolerated and only some induce neurotoxicity. In addition, these studies suggest almost all Eg5 inhibitors as more effective in combination with other anti-tumor drugs currently used in clinical therapy (because they enhance other drug activity) rather than in monotherapy where they highlighted limited clinical response [99].

In 1999 Mayer et al identified a new specific cell permeable Eg5 inhibitor able to cause the monopolar spindle assembly, called monastrol [104].

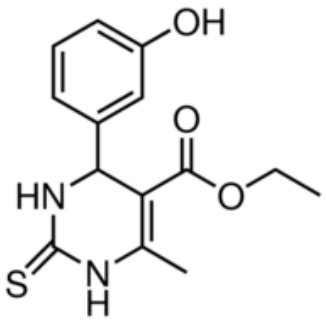

Figure 10: Chemical structure of monastrol.

Its binding site is a hydrophobic pocket among alpha-helix 3 and loop 5 in Eg5 motor domain leading to lock the loop into ADP bound-like arrangement. Monastrol does not compete with microtubule or ATP binding, but it arrests microtubule-stimulated ADP release. Besides, in one study monastrol has been demonstrated to be a promoter of ATP hydrolysis step turnaround [105].

This compound demonstrated anti-tumor activity in several cell lines, but poor clinical efficacy because of its weak inhibition activity and its high concentration required to induce cell death that could be reflected into toxic side effects [106].

2. Aim of the study

Human head and neck squamous cell carcinomas (HNSCC) are a group of tumors representing the sixth most frequent cancer worldwide [1]. This type of neoplasm can be located into diverse regions of the oral cavity, oropharynx, hypopharynx and larynx [3].

Almost 50% of patients have a survival rate of fewer than 5 years, more than half a million new cases are diagnosed per year [1] and the HNSCC incidence continues to rise [4]. In addition to deaths directly caused by the tumor, HNSCC have also the second-highest rate of survivor suicide because of compromised quality of life and psychological problems resulting from cancer development [7].

Furthermore, HNSCC is characterized by poor prognosis, mainly due to metastasis [107][108]. Distant metastasis detection has a prognostic value in HNSCC, showing a high mortality rate [2]. This is attributed to poor responses to chemotherapy by metastatic disease [109][110].

Frequently drug resistance is revealed in HNSCC and, on the other hand, the poor response to chemotherapy requires the use of radiation and surgical interventions that often lead to a permanent impairment of oral functions [111][112]. To sum up, despite several drugs show promising anti-cancer activity, new therapeutic options are still urgently needed.

Anti-mitotic agents are hopeful anti-cancer drugs because these compounds lead to apoptotic cell death and consequent tumor regression. This is due to their activities during the cell cycle, by stopping it at the G2/M phase [57].

For these reasons we first tested some novel synthesized amino-pyrimidine compounds not only on HNSCC, but also on other cancer cell lines, to evaluate their anti-neoplastic activity on a wider range of tumor types. These compounds are structurally derived from an amino-pyrimidine molecule that has previously demonstrated an important ability to inhibit proliferation, induce apoptosis, and block the cell cycle at the G2/M stage on different cancer types [113].

Consequently, we expected these new compounds to be effective in these fields too, but our goal was to verify that their effect could be extended to HNSCC, to tongue and pharynx squamous cell carcinomas.

In the second report, we decided to analyse the anti-tumor effects of another neo-synthesized molecule, RDS 60, structurally related to nocodazole.

Nocodazole target is the beta tubulin subunit. Tubulin binding with compound inhibits the heterodimers formation [82][83], thus leading to the impossibility of starting mitosis due to abnormal mitotic spindle assembly [84][85].

In the third report, we studied one of the most effective kinesin Eg5 inhibitors, K858. This molecule has already been demonstrated to have significant anti-neoplastic activity on different tumors, such as prostate and breast carcinomas, melanoma and glioblastoma [114][115][116][117][118].

Kinesin Eg5 inhibition prevents ordinary microtubule organization to the mitotic spindle, leading to the formation of a monopolar spindle called "monoaster". The final effect is a mitotic arrest and then apoptotic cell death [97].

In both these two last reports, we evaluated the activity of RDS 60 and K858 on proliferation, cell cycle regulation and apoptosis induction in HNSCC cell lines. We also analysed these two compounds efficacy on inhibiting invasiveness and epithelial-to-mesenchymal transition in the same HNSCC cell lines.

3. Materials and methods

3.1 General and chemistry

Melting points were determined on a Bobby Stuart Scientific SMP1 melting point apparatus (Bibby Scientific, Stone, UK) and are uncorrected. Compound purity was always >95% as determined by combustion analysis. Analytical results agreed to within ±0.40% of the theoretical values. IR spectra were recorded on a PerkinElmer Spectrum-One spectrophotometer (Perkin Elmer, Shelton, CT, USA). 1H NMR spectra were recorded at 400 MHz on a Bruker AC 400 Ultrashield 10 spectrophotometer (400 MHz) (Bruker, Billerica, MA, USA). Dimethyl sulfoxide-d6 99.9% (CAS 2206-27-1) and deuterochloroform 98.8% (CAS 865-49-6) of isotopic purity (Aldrich, St. Louis, MO, USA) were used. Column chromatographies were performed on silica gel (Merck, Darmstadt, Germany; 70−230 mesh) and on aluminum oxide (Merck; 70–230 mesh). All compounds were routinely checked on TLC by using aluminum-baked silica gel plates (Fluka, Honeywell, Charlotte, NC, USA; DC-Alufolien Kieselgel 60 F254) or TLC aluminum oxide 60 F254 basic (Merck). Developed plates were visualized by UV light. Solvents were reagent grade and, when necessary, were purified and dried by standard methods. Concentration of solutions after reactions and extractions involved the use of a rotary evaporator (Büchi, Flawil, Switzerland) operating at a reduced pressure (ca. 20 Torr). Organic solutions were dried over anhydrous sodium sulphate (Merck). All solvents were freshly distilled under nitrogen and stored over molecular sieves for at least 3 h prior to use.

For the first report:

General Procedure A (GP-A) for the Synthesis of Derivatives 4a–d, f: to a solution of commercially available 2,6-dichloropyrimidine-4-amine (30 mmol) in anhydrous 2-methoxyethanol (100 mL), a suitable aniline (30 mmol) was added, and the reaction was stirred vigorously under reflux overnight. The solvent was reduced under vacuum, and the crude product was diluted with chloroform (300 mL). The organic layer was washed with water (300 mL), 1N HCl (250 mL) and saturated NaCl solution (3 × 300 mL), dried over Na2SO4 and concentrated under reduced pressure. The raw product was purified by column chromatography on silica gel (dichloromethane: methanol 98:2 as eluent).

The structures of compound 4a and its regioisomer was confirmed by means of 2D-NMR.

General Procedure B (GP-B) for the Synthesis of Derivatives 1a and 1b: a mixture of an appropriate 2-substituted pyrimidine 4a–b (1 mmol), N1, N1 -diethylpropane-1,3-diamine (1 mmol) and anhydrous K2CO3 (2.5 mmol) in anhydrous DMF (0.8 mL) was irradiated with microwave at 150 ◦C for 30 min. After cooling, chloroform was added (5 mL) and the precipitate that formed was filtered and washed with ethyl acetate (7 mL). The organic layers were combined and evaporated under reduced pressure. The raw was quenched with 1N HCl (8 mL) and washed with chloroform (10 mL), then 1N NaOH was added until pH = 14 was reached and the aqueous layer was extracted with chloroform (2 × 20 mL). The organic layer was dried over Na2SO4 and concentrated under reduced pressure to give a dark brown oil that was purified by column chromatography on aluminium oxide (chloroform/methanol 9:1 as eluent).

General Procedure C (GP-C) for the Synthesis of Derivatives 1c, d, f, g: in a microwave vial, the appropriate 2-substitued pyrimidine 4a, c, d, f (1 mmol) was dissolved in isopropanol (1 mL), DIPEA (1.2 mmol) and appropriate amine (1.1 mmol) was added. The vial was sealed and heated by microwave at 150 ◦C for 3 h. After cooling, chloroform was added (10 mL) and the organic layer was quenched with 1N HCl (8 mL). Then 1N NaOH was added until pH = 12 was reached and the aqueous layer was extracted with chloroform (2 × 20 mL). The organic layer was washed with brine (2 × 20 mL), dried over Na2SO4 and concentrated under reduced pressure to give a dark brown oil that was purified by column chromatography on aluminium oxide.

General Procedure D (GP-D) for the Synthesis of Derivatives 2a, b,d–f: to a well-stirred suspension of NaH 60% (0.562 mmol or 0.843 mmol for hydrochloride salt 1e-HCl) in anhydrous DMF (2 mL) derivatives 1a,b,d–f (0.281 mmol), and the 4- fluorobenzyl bromide (0.320 mmol) was added at 0 ◦C under argon atmosphere. The reaction was stirred for the proper time at room temperature and then quenched with crushed ice. The mixture was extracted with chloroform (3 × 4 mL) and the organic extracts were collected, washed with brine (4 × 2 mL), dried over Na2SO4 and evaporated at reduced pressure [16]. The crude products were purified by column chromatography Molecules 2021, 26, 771 10 of 15 (Al2O3 or SiO2, see experimental section) yielding the pure derivative 2a, b, d–f.

For the second report: melting point (◦C), recrystallization solvent, yield (%), chromatographic system, IR, 1H NMR, formula, Mr and analysed elements for intermediates 1–5 and derivative RDS 60 agreed with the ones previously described [119]. RDS 60 samples used for biological evaluation were 99% pure as determined by elemental analysis.

(3,4-Dinitrophenyl) methanol: A solution of AlCl3 (3.77 g; 28.28 mM) in THF dry (4.6 mL) was added dropwise into a solution of commercially available 3,4-dinitrobenzoic acid (5 g; 23.57 mM) and NaBH4 (3.21 g; 84.85 mM) in THF dry (46 mL) at 0 ◦C within 20 min. The reaction was stirred at 25 ◦C for 1 h (h) and for 2 h to reflux and then poured into ice-cold water (115 mL). The pH was adjusted to 7 with 1 N HCl and the mixture was extracted with ethyl acetate (3 × 50 mL). The collected extracts were washed with brine (3 × 100 mL) and dried. Removal of the solvent furnished crude residue that was washed with ethyl acetate to discard the boron salt, yielding intermediate 1 (3.37 g: 72.1%) as a yellow solid.

4-(Chloromethyl)-1,2-dinitrobenzene: To a solution of compound 1 (16.27 g; 81.85 mM) in CHCl3 (126 mL) was added PCl5 (6.63 g; 31.85 mM) portion-wise at 0 ◦C within 15 min. The reaction mixture was stirred at 0 ◦C for 15 min and at 25 ◦C for 2.5 h Pharmaceuticals 2021, 14, 564 11 of 14 and then poured into ice-cold water. The organic layer was washed with 5% w/v Na2CO3 (3 × 100 mL) and with NaClss (3 × 100 mL) and dried. Removal of the solvent furnished the crude compound 2 that underwent the following step without further purification.

(3,4-Dinitrophenyl) methenamine (3): compound 3 was prepared according to the literature [80]. 1-(3,4-Dinitrobenzyl)-1H-pyrrole (4). Compound 4 was prepared according to the literature [80]. (4-((1H-pyrrol-1-yl) methyl) benzene-1,2-diamine (5). Compound 5 was prepared according to the literature [80]. Ethyl (5-((1H-pyrrol-1-yl) methyl)-1H-benzo[d]imidazol-2-yl) carbamate (RDS 60). RDS 60 was prepared according to the literature [119]. Analytical data are herein reported.

For the third report: solvents were used without further purification. Where mixtures of solvents are specified, the stated ratios are volume: volume. Reagents and standard drug (Docetaxel) were used directly as supplied by Sigma Aldrich Italy. Column chromatography was carried out using Sigma Aldrich silica gel (high purity grade, pore

size 60 Å, 230-400 mesh particle size). Analytical thin layer chromatography was carried out on Sigma Aldrich silica gel on TLA aluminum foils with fluorescent indicator 254 nm. Visualization was carried out under ultra-violet irradiation (254 nm). NMR spectra were recorded on a Bruker AV400 (^{1}H: 400 MHz, ^{13}C: 101 MHz). Coupling constants J are valued in Hertz (Hz). Chemical shifts are expressed as d units (parts per millions), based on appearance rather than interpretation, and are referenced to the residual not deuterated solvent peak. IR spectra were recorded on a FT-IR Perkin Elmer Spectrum One equipped with ATR system. Absorption maxima (n_{max}) are reported in wavenumbers (cm^{1}). All melting points were measured on a Stuart melting point apparatus SMP1 and are uncorrected. Temperatures are reported in C. Where given, systematic compound names are those generated by Chem-Draw Ultra 8.0 following IUPAC conventions.

Different carbonyl compounds were reacted with thio-semicarbazide (1.0 eq.) in ethanol (50 mL) with catalytic amounts of acetic acid for 12-72 h at room temperature. The mixture was filtered and the solid washed with petroleum ether and n-hexane and purified by column chromatography (ethyl acetate: hexane) to obtain the corresponding thiosemicarbazone in high yields (75e99%). Different Eg5 inhibitors were synthesized, and the most effective one was chosen for further investigation.

3.2 Cell culture and treatments

In our first report human tumor cell lines utilized were: glioblastoma multiforme U-87 MG, triple-negative breast cancer MDA-MB231, colon carcinoma HT-29, tongue squamous cell carcinoma CAL 27 (CRL-2095, ATCC, Manassas, VA, USA) and pharynx squamous cell carcinoma FaDu (HTB-43, ATCC, USA), all of which obtained from the American Type Culture Collection (Manassas, USA). In addition, human dermal fibroblast primary cultures (HF) used as control of non-transformed cells, had been previously established in our laboratory [120]. The cells were grown at 37 ◦C and 5% CO2 in Dulbecco's modified Eagle's medium or RPMI 1640 medium supplemented with 10% fetal bovine serum, 2 mM glutamine and 50 U/mL penicillin-streptomycin (Sigma-Aldrich). All compounds were solubilized in dimethyl sulfoxide (DMSO) (Sigma) for a 10 mM stock solution and utilized to final concentrations from 100 nM to 60 µM for 24 and 48 h. Control cells were treated with equivalent amounts of DMSO in every experiment.

For the second report the following cell lines were utilized: tongue HNSCC CAL 27 (CRL-2095, ATCC, Manassas, VA, USA), pharynx HNSCC FaDu (HTB-43, ATCC, USA), human keratinocytes HaCaT (ATCC, USA) and human dermal fibroblasts HF previously established and characterized in our laboratory [113]. Mycoplasma testing was done for all cell lines at the beginning of the study. Cells were grown in RPMI 1640 medium with 10% fetal calf serum (FCS), 2 mM glutamine and 50 U/mL penicillin-streptomycin (Sigma-Aldrich). The compound RDS 60 was solubilized in dimethyl sulfoxide (DMSO) (Sigma) for a 10 mM stock solution and utilized to final concentrations from 100 nM to 10 µM for 24 and 48 h. Control cells were treated with equivalent amounts of DMSO in every experiment.

For the third report three HNSCC cell lines were utilized: tongue carcinoma CAL 27 (CRL-2095, ATCC, Manassas, VA, USA) and SCC-15 and pharynx carcinoma FaDu (HTB-43, ATCC, USA). Cells were grown in RPMI 1640 medium with 10% fetal calf serum (FCS), 2 mM glutamine and 50 U/mL penicillin-streptomycin (Sigma-Aldrich). K858 was synthesized, characterized and utilized as previously described [115]. K858 was solubilized in dimethyl sulfoxide (DMSO) (Sigma-Aldrich) at 1 mM stock solution. YM155 (Selleckem) was solubilized in DMSO at 10 µM stock solution and used 10 nM. Untreated control cells were treated with equivalent amounts of DMSO in every experiment.

3.3 Cytotoxicity assay

To determine cytotoxicity, a sulforhodamine-B colorimetric assay was performed: 5×10^3 cells were plated in 96-well plates, grown for 24 h and then treated for 24 and 48 h with different concentration of compound reported in first report or different concentration of RDS 60 in the second report or several concentrations of K858 in the third one. Cells were then fixed with 50% trichloroacetic acid for 1 h at 4 ◦C and stained for 30 min at room temperature (RT) with 0.4% sulforhodamine-B in 1% acetic acid. Excess dye was removed by washing four times with 1% acetic acid. Protein-bound dye was dissolved in 10 mM Tris pH 10 and optical density was determined at 510 nm using a microplate reader.

3.4 Flow cytometry analysis

Cells were grown on 60-mm plates for 24 h and then treated with 1 µM (for cell cycle analysis) or 2 µM (for apoptosis analysis) RDS 60 or equivalent amounts of DMSO for 24 h in the second report, while with 2 µM K858 for 24 h in the third report. Detached and adherent cells were harvested by trypsinization and washed twice with cold PBS. For apoptosis and necrosis rate quantification, the cells were double stained with Annexin V-APC (allophycocyanin) and 7AAD (7-amino-actinomycin) in Ringer solution containing 5 mM CaCl2 for 1 h at 4 ◦C according to the manufacturer's instructions (BD Biosciences, Apoptosis kit, Franklin Lakes) and analysed by a fluorescence activated cell sorting cytofluorimeter (FACS) FACS Calibur (BD Biosciences) and by the Cell-Quest Pro software version 5.1 (BD Biosciences). The analysis was performed in triplicate for each cell line and the mean values were presented. For cell cycle analysis, the cells were fixed in 70% ethanol overnight at 4 ◦C and then were rinsed twice with PBS and incubated with 50 µL of RNAse (100 µg/mL, Sigma, Kawasaki, Japan in the second report/10 mg/mL RNase Sigma Aldrich for the third one) to ensure that only DNA was stained, and 200 µL of propidium iodide (PI) (50 µg/mL, Sigma) in the second report and 1 mg/mL propidium iodide (Sigma Aldrich) at RT for 2 h in the dark for the third one. Cell staining analysis was performed using the FACS CantoII equipped with 488 nm laser and DIVA Software (BD Biosciences). The cells were first gated using a forward vs. side scatter (FSC vs. SSC) strategy and upon 488 nm laser excitation, then Annexin V-APC and PI fluorescence was detected above 580 nm. Data were analysed using Flow Jo software (Flow Jo LLC, Ashland).

3.5 Western blotting

Cells were grown in 100-mm plates for 24 h and treated with 2 µM RDS 60 or 2.5 µM K858 equivalent amounts of DMSO for 24 h. Cells were then scraped in lysis buffer composed of 1% Triton, 0.1% sodium dodecyl sulphate, 150 mM NaCl, 50 mM Tris HCl pH 7.4, 2 mM EDTA with protease inhibitor cocktail (Roche Applied Science) for 30 min at 4 ◦C. Lysates were centrifuged at 16,000× g for 15 min at 4 ◦C and the supernatant was collected. Protein concentration was evaluated using Protein Concentration Assay (Bio-Rad Laboratories).

Protein lysates (50–100 µg) were separated by molecular weight with 10, 12 or 14% SDS-PAGE and then transferred onto nitrocellulose membranes. Membranes were blocked for 1 h at RT in 5% non-fat dry milk and incubated with primary antibodies opportunely diluted in PBS-Tween overnight at 4 ◦C, then washed in Tris-buffered saline with 0.1% Tween-20 and incubated with horseradish-peroxidase-conjugated-anti-mouse/rabbit-IgG (1:5000; Sigma-Aldrich) for 1 h at RT. Filters were finally developed using enhanced chemiluminescence (Super Signal West Pico Chemiluminescence Substrate; Thermo Fisher Scientific) using Kodak X-Omat films (Kodak, Rochester, NY, USA).

Primary antibodies used in the second report were: mouse anti-poly (ADP-ribose)-polymerase (PARP-1) (diluted 1:500; Santa Cruz Biotechnology); mouse anti-cleaved-caspase 8 (diluted 1:500; Cell Signaling Technology); mouse anti-caspase 9 (diluted 1:500; Cell Signaling Technology); mouse anti-B-cell-lymphoma-2 (Bcl-2) (diluted 1:200; Santa Cruz Biotechnology); rabbit anti-Bcl-2-associated-X-protein (Bax) (diluted 1:250; Santa Cruz Biotechnology); rabbit anti E-cadherin (1:1000 diluted; GeneTex); rabbit anti N-cadherin (1:1000 diluted; GeneTex); rabbit anti cyclin B1 (1:500 diluted; Elabscience, USA); rabbit anti-tubulin (diluted 1:4000; Immunological Sciences).

Primary antibodies used in the third report were: rabbit anti cyclin B1 (1:500 diluted; Elabscience, USA); mouse anti-poly (ADP-ribose)-polymerase (PARP-1) (diluted 1:500; Santa Cruz Biotechnology, TX, USA); mouse anti-caspase 8 (diluted 1:500; Cell Signaling Technology, MA, USA); mouse anti-caspase 9 (diluted 1:500; Cell Signaling Technology); mouse anti-B-cell-lymphoma-2 (Bcl-2) (diluted 1:200; Santa Cruz Biotechnology); rabbit anti-Bcl-2-associated-X-protein (Bax) (diluted 1:250; Santa Cruz Biotechnology); rabbit anti E-cadherin (1:1000 diluted; GeneTex); rabbit anti N-cadherin (1:1000 diluted; GeneTex); rabbit anti MMP-1 (1:500 diluted; Biomol); rabbit anti MMP-2 (1:1000 diluted; GeneTex); rabbit anti-tubulin (diluted 1:4000; Immunological Sciences).

Experiments were performed in duplicate or triplicate, the bands from the blots were quantified using ImageJ v.1.48 software (National Institutes of Health, Bethesda, MD, USA), the mean values were calculated and expressed as densitometric units (DU).

3.6 Immunofluorescence

The cells were grown directly on Labteck chamber slides (Nunc) for 24 h and then used untreated or treated for 24 h with 1 μM RDS 60 or 1 μM K858. Cells were washed with PBS with Ca/Mg (washing buffer) and fixed with 4% buffered paraformaldehyde (Sigma Aldrich) for 20 min at 4 °C, then permeabilized with PBS, 5% FCS, 0.5% TritonX100 for 30 min at RT and incubated for 1 h at RT with the primary monoclonal antibody to beta-tubulin (1:100 diluted; Immunological Sciences). Alternatively, in the second report cells were permeabilized with 0.1% TritonX100 for 10 min to RT, incubated with 3% BSA for 1 h at RT and incubated with the primary rabbit polyclonal antibody to cyclin B1 in 0.1% BSA (1:200 diluted; Elabscience) overnight at 4 ◦C. Cells were washed twice with washing buffer and incubated with the secondary anti-mouse antibody FITC conjugated (1:400 diluted; Molecular Probes) for 1 h at RT. Cells were washed twice with washing buffer and DNA was stained with Hoechst for 15 min to RT. The slide was mounted with ProLong-Antifade (Life Technologies) and analysed by a fluorescence microscope (Olympus BX52). Image acquisition and processing were conducted by IAS 2000 software.

3.7 Invasion assay

Invasion assay was performed with Bio Coat Matrigel Invasion Chambers (Corning), consisting of inserts with an 8 μm pores size membrane that was previously treated with Matrigel matrix. For invasion assay 2.5×10^{5}/mL cells were plated in serum-free medium plus vehicle DMSO or in serum- free medium plus 10 μM RDS 60 for the second report or 1 μM K858 for the third report in the insert chamber, the lower chamber instead contained only complete medium (with serum). After 16 h of culture at standard conditions, the inserts were washed with PBS with Ca/Mg and fixed by 100% methanol for 20 min at 4 °C, then washed twice with PBS with Ca/Mg and stained for 20 min at RT with hematoxylin.

The inserts were then mounted on a slide with glycerol and the cells that migrated through the filter pores to the lower side of the membrane were counted with an optical microscope (Olympus BX52). Imagine acquisition and processing were conducted by IAS 2000 software.

3.8 Statistical analysis and graphic programs

All results were analysed by ANOVA, and the significance was evaluated by the Tukey HSD post hoc test (Honestly Significant Difference). All figures were elaborated with Adobe Photoshop CS5 and all graphs with Graph Pad Prism 5.0.

4. Results 1° report

Synthesis and biological evaluation of new pyrimidine derivatives as anticancer agents.

Madia VN; Nicolai A; Messore A; De Leo A; Ialongo D; Tudino V; Saccoliti F; De Vita D; Scipione L; Artico M; Taurone S; Taglieri L; Di Santo R; Scarpa S; Costi R.
Anticancer Agents. Molecules 2021, 26, 771.
https://doi.org/10.3390/molecules26030771

Discovery of a pyrimidine compound endowed with antitumor activity.

Taglieri L; Saccoliti F; Nicolai A; Peruzzi G; Madia VN; Tudino V; Messore A; Di Santo R; Artico M; Taurone S; Salvati M; Costi R; Scarpa S.
Invest. New Drugs 2020, 38, 39–49.
https://doi.org/10.1007/s10637-019-00762-y

Recently, the groups of Prof. Roberta Costi and Prof. Roberto Di Santo at the Department of Drug Chemistry and Technologies, Sapienza University, have synthesized a new aminopyrimidine compound named RDS 3442. Therefore, our group tested in vitro the biological activity of this new molecule on three different human cancer types (glioblastoma multiforme, triple-negative breast cancer and colon adenocarcinoma) and found it can be an innovative anti-tumor agent because it inhibits cell proliferation, leads to cell cycle arrest at G0/G1 phase (20 μM) through the p21 and p27 up-regulation (two G1-checkpoint cyclin-dependent kinases inhibitors) and finally induces apoptosis (30–50 μM) [113].

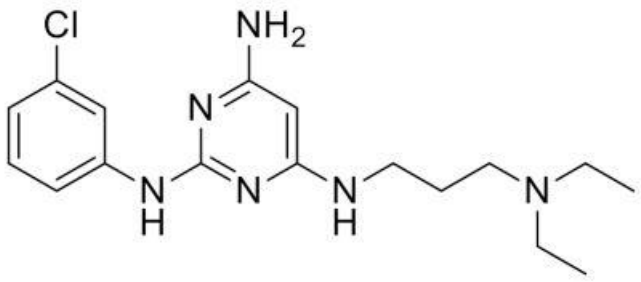

Figure 11: Chemical structure of RDS 3442 (compound 1a).

Given these promising results, new aminopyrimidine derivatives structurally linked to RDS 3442 (1b–g, 2a–f and 3) were synthesized and analysed. All these compounds were devised by putting in place substitutions in position 6 of the pyrimidine core and/or on the 2-aniline ring of compound 1a, but compound 3 was found as a by-product during a nucleophilic aromatic substitution.

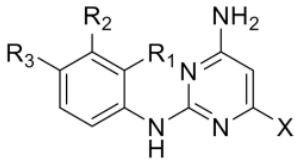

1a–g

1a X=3-(diethylamino)propyl-amino; R_1 = H; R_2 = Cl; R_3 = H
1b X= 3-(diethylamino)propyl-amino; R_1 = H R_2= F R_3= H
1c X= 3-(diethylamino)propyl-amino; R_1 = H; R_2 = OCH_3; R_3 = H
1d X= 3-(diethylamino)propyl-amino; R_1 = H; R_2 = NO_2; R_3 = H
1e-HCl X=dipropylamino; R_1 = H R_2 = Cl R_3 = H
1e X=dipropylamino; R_1 = H; R_2 = Cl; R_3 = H
1f X=dipropylamino; R_1 = F; R_2 = H; R_3 = Cl
1g X=4-methylpiperazin-1-yl; R_1 = H; R_2 = Cl; R_3 = H

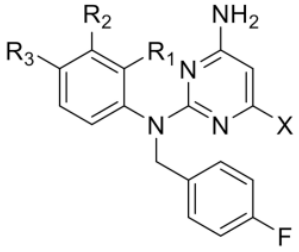

2a–f

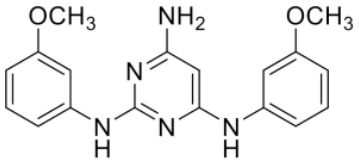

3

2a X = 3-(diethylamino)propyl-amino; R_1 = H; R_2 = Cl; R_3 = H
2b X = 3-(diethylamino)propyl-amino; R_1 = H R_2= F R_3= H
2c X = 3-(diethylamino)propyl-amino; R_1 = H; R_2 = OCH_3; R_3 = H
2d X = 3-(diethylamino)propyl-amino; R_1 = H; R_2 = NO_2; R_3 = H
2e X = dipropylamino; R_1 = H R_2 = Cl R_3 = H
2f X = dipropylamino; R_1 = F; R_2 = H; R_3 = Cl

Figure 12: Structures of novel designed aminopyrimidine derivatives, 1a–g, 2a–f and 3.

These new compounds were analysed by our group for their possible anti-neoplastic role on the following human cell lines:

- MDA-MB231, triple-negative breast cancer.
- HT-29, colon carcinoma.
- U-87 MG, glioblastoma multiforme.
- CAL 27, tongue squamous cell carcinoma.
- FaDu, pharynx squamous cell carcinoma.

These human tumor cell lines were treated for 24 and 48 h with 10, 20, 30, 40, 50 and 60 μM of each molecule. Then we analysed the resulted alterations on cellular replication by sulforhodamine B proliferation test.

To evaluate a potential cytotoxicity on somatic human not transformed cells we performed a proliferation assay also on human dermal fibroblasts (HF) at the same concentrations revealed to be active on tumor cells, but only when a compound demonstrated significant

anti-proliferative efficacy at tolerable concentrations (lower than 30 µM). The 50% cytotoxic concentration (CC_{50}) on HF at 48 h was calculated and reported (Table 1,2).

We evaluated the median values from three different proliferation assays of all compounds for each cell line and calculated and reported the EC_{50} at 24 and 48 h in tables 1-2. In this study is also reported the anti-proliferative activity of each compound also compared with compound 1a, RDS 3442.

Cpd	EC_{50} (µM) [1]					CC_{50} (µM) [2]
	HT-29	U-87 MG	MDA-MB231	CAL27	FaDu	HF
1b	29.8 (48 h) ± 3.2	47.3 (48 h) ± 3.6	35.7 (48 h) ± 3.2	20.3 (48 h) ± 1.8	43.4 (48 h) ± 3.9	88 (48 h) ± 9.0
1c	57 (48 h) ± 2.4	68 (48 h) ± 5.0	70.5 (48 h) ± 6.0	57 (48 h) ± 4.0	71 (48 h) ± 5.6	nd [3]
1d	40.4 (48 h) ± 4.8	54.9 (48 h) ± 4.8	49.2 (48 h) ± 3.5	35.3 (48 h) ± 3.9	46.8 (48 h) ± 5.0	97 (48 h) ± 13.0
1e-HCl	29.3 (48 h) ± 1.7	36.6 (48 h) ± 2.9	50.2 (48 h) ± 4.5	30.3 (48 h) ± 2.4	39.8 (48 h) ± 4.0	76 (48 h) ± 5.5
1e	28.5 (48 h) ± 1.9	45.3 (48 h) ± 3.8	34.2 (48 h) ± 2.5	24.7 (48 h) ± 1.8	29.7 (48 h) ± 3.2	68 (48 h) ± 5.2
1f	50 (48 h) ± 3.3	75 (48 h) ± 4.9	58 (48 h) ± 6.1	55 (48 h) ± 5.7	67 (48 h) ± 4.9	98 (48 h) ± 8.0
1g	60 (48 h) ± 5.8	82 (48 h) ± 7.0	55 (48 h) ± 3.7	60 (48 h) ± 6.2	87 (48 h) ± 7.0	nd [3]
3	28.2 (24 h) ± 1.4 11.7 (48 h) ± 0.9	22.9 (48 h) ± 2.5	10.2 (48 h) ± 1.5	20.3 (24 h) ± 2.8 10.4 (48 h) ± 0.8	42.1 (24 h) ± 3.6 19.7 (48 h) ± 2.0	65 (48 h) ± 4.1
1a	51.8 (48 h) ± 4.2	75.2 (48 h) ± 6.2	34.8 (48 h) ± 2.8	54.2 (48 h) ± 4.8	69.3 (48 h) ± 5.8	73.6 (48 h) ± 6.0

[1] Half maximal effective concentration (µM) on five different cell lines at 24 and 48 h ± SD. [2] Half maximal cytotoxic concentration (µM).
[3] not determined.

Table 1: Cytotoxicity and anti-tumor activities of the newly synthesized compounds 1b–g and 3 in comparison with reference compound 1a.

Cpd	EC_{50} (µM) [1]					CC_{50} (µM) [2]
	HT-29	U-87 MG	MDA-MB231	CAL27	FaDu	HF
2a	10.2 (24 h) ± 0.6 5.4 (48 h) ± 0.4	22.0 (24 h) ± 1.3 7.5 (48 h) ± 0.6	18.0 (24 h) ± 0.7 7.9 (48 h) ± 0.8	9.7 (24 h) ± 0.6 4.3 (48 h) ± 0.5	26.2 (24 h) ± 3.2 8.5 (48 h) ± 1.1	50.2 (48 h) ± 3.8
2b	20.2 (24 h) ± 1.9 10.4 (48 h) ± 0.8	17.7 (48 h) ± 1.2	7.3 (48 h) ± 0.5	5.1 (48 h) ± 0.3	23.8 (48 h) ± 2.1	54.7 (48 h) ± 4.2
2c	34.7 (24 h) ± 2.8 18.3 (48 h) ± 1.2	19.8 (48 h) ± 1.4	27.2 (48 h) ± 1.8	14.9 (48 h) ± 1.1	18.2 (48 h) ± 1.3	50.3 (48 h) ± 3.7
2d	25.2 (24 h) ± 2.0 12.7 (48 h) ± 1.1	30.1 (48 h) ± 2.4	17.3 (48 h) ± 1.9	10.3 (48 h) ± 0.9	20.5 (48 h) ± 2.3	55.2 (48 h) ± 4.9
2e	65.2 (48 h) ± 5.0	72.4 (48 h) ± 3.8	60.8 (48 h) ± 7.0	59.3 (48 h) ± 4.7	84.4 (48 h) ± 5.0	nd 3
2f	30.0 (48 h) ± 1.5	67.0 (48 h) ± 5.0	58.3 (48 h) ± 6.5	45.4 (48 h) ± 1.8	75.3 (48 h) ± 6.9	nd 3
1a	51.8 (48 h) ± 4.2	75.2 (48 h) ± 6.2	34.8 (48 h) ± 2.8	54.2 (48 h) ± 4.8	69.3 (48 h) ± 5.8	73.6 (48 h) ± 6.0

[1] Half maximal effective concentration (µM) on five different cell lines at 24 and 48 h ± SD. [2] Half maximal cytotoxic concentration (µM).
[3] not determined.

Table 2: Cytotoxicity and anti-tumor activities of the newly synthesized compounds 2a–f in comparison with reference compound 1a.

These following results can be assumed from tables 1 e 2:

- Series 2 derivates induce a significant decrease of cell proliferation in all cell lines, more than series 1.
- Series 2 compounds show a cytotoxic activity on normal fibroblasts but not significative by considering the anti-cancer activity concentrations.
- Four of six molecules in series 2 are functioning against all tested cell lines with concentrations lower than 20 µM at 48 h of treatment, while only one compound within series 1 is active at 20 µM after 48 h of treatment, but just on CAL 27 line.
- Among series 1 derivates, 1e is the most active compound, showing higher potency than compound 1a on each cell line and reporting EC_{50}s: 25- 45 µM at 48 h of treatment and no cytotoxic activity on HF cells up to 60 µM. Only on CAL 27, it was slightly exceeded by derivative 1b.
- Derivative 3 is active at concentrations up to 20 µM after 48 h of treatment similarly to series 2 compounds.
- HT-29 and CAL 27 are more sensitive to both series 1 and 2 than the other cell lines.

The most active derivative was 2a with EC_{50}s = 10–26 µM at 24 h and 5–8 µM at 48 h of treatment. For this reason, we reported below its cell viability graph for all cell lines. (Fig. 13)

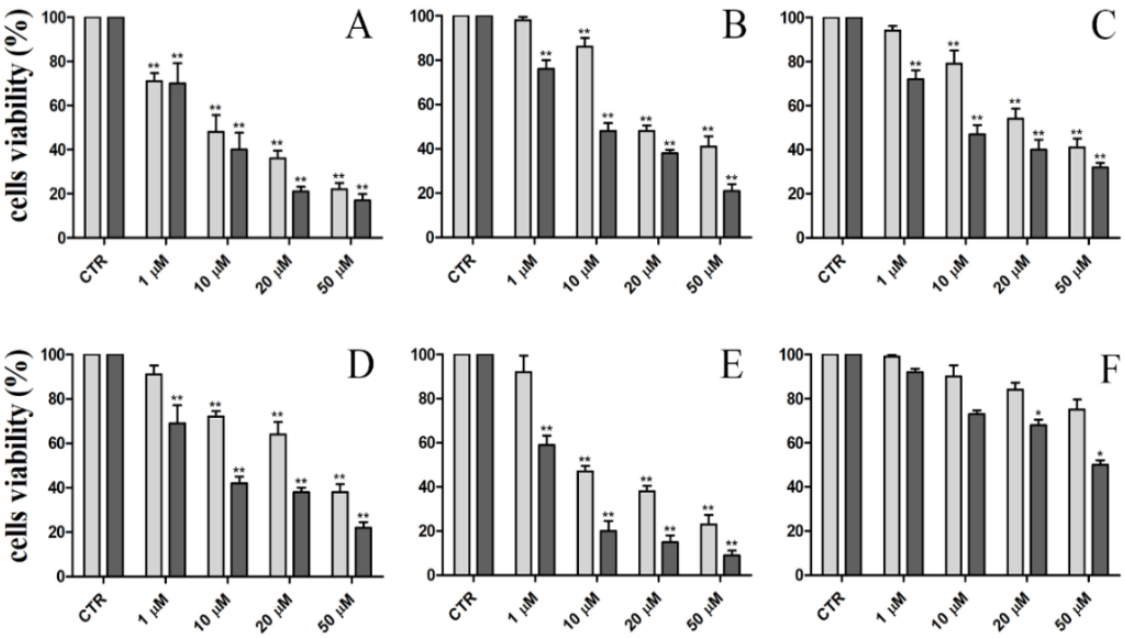

Figure 13: Cell viability of HT-29 (A), MDA-MB231 (B), U-87 MG (C), FaDu (D), CAL 27 (E), HF (F) untreated (CTR) and treated with compound 2a at 1, 10, 20, 50 µM for 24 h (light grey) and 48 h (dark grey). The values are expressed as percentages of alive cells ± SD. * $p < 0.01$; ** $p < 0{,}001$.

5. Discussion 1° report

Fight against cancer is still an important medical issue. Despite numerous molecules are currently used in therapy, several patients are not able to overcome the disease; among these triggers, insensitivity to therapy and drug resistance are found [63][111].

For this reason, developing and validating new anti-cancer approaches is strongly required. Starting from promising results obtained by RDS 3442 molecule, we wanted to exploit its chemical characteristics to develop new compounds. New synthesised aminopyridine derivatives were evaluated as potential new anti-tumor agents by a proliferation test which allowed us to highlight their potential inhibition on transformed cell replication.

RDS 3442 was found to be a good replication inhibitor and cell cycle negative regulator on glioblastoma multiforme, triple-negative breast cancer and colon adenocarcinoma cell lines [113]. Thus, we aimed to develop new compounds trying to improve the RDS 3442 chemical structure and increase its anti-tumor activity.

We used various types of cancers to test their greater therapy application. We treated head and neck squamous cell carcinomas because the HNSCC incidence continues to rise [4] and drug resistance is frequently detected in this type of cancer [4].

In this study we found that the 2a compound, N-benzyl counterpart of RDS 3442, was the best molecule with the highest rate of proliferation inhibition in all tumor cell lines.

These described results suggest that it is possible to improve anti-cancer activity by providing to aminopyrimidine core different substituents in positions 2 and 6.

However, further studies are necessary to investigate their action mechanism. For now, we have only put bases for their successive deepened evaluation as potential anti-neoplastic agents.

6. Results 2° report

Anti-tumoral effects of a (1H-Pyrrol-1-Yl) Methyl-1H-Benzoimidazole carbamate ester derivative on head and neck squamous carcinoma cell lines.

Nicolai A; Madia VN; Messore A; De Vita D; De Leo A; Ialongo D; Tudino V; Tortorella E; Scipione L; Taurone S; Pergolizzi T; Artico M; Di Santo R; Costi R; Scarpa S.

Pharmaceuticals 2021, 14, 564.

https://doi.org/10.3390/

More than a few studies suggested benzimidazole as the most important heterocycle since its cytotoxic activity against several tumor types [80][81]. Numerous benzimidazole-based drugs have been analysed in pre-clinical and clinical studies revealing stimulating anti-cancer activity. These compounds bind to the colchicine binding site in tubulin subunit [121]. Among this class, nocodazole targets beta-tubulin subunit, avoiding its link with alpha-tubulin subunits; however, contrary to colchicine, the nocodazole binding to tubulin could be quickly reversible [122].

Thus, the groups of Prof. Roberta Costi and Prof. Roberto Di Santo at the Department of Drug Chemistry and Technologies, Sapienza University, performed a new compound structurally correlated with nocodazole, named RDS 60. This molecule is a (1H-pyrrol-1-yl) methyl-1H-benzimidazole derivative, and our research aimed to evaluate RDS 60 efficacy as anti-cancer agent against human head and neck squamous cell carcinomas (HNSCC).

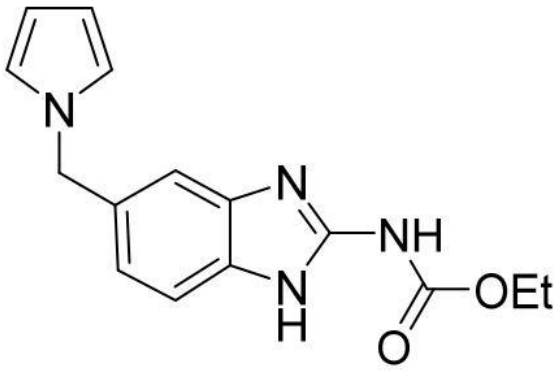

Figure 14: Chemical structure of RDS 60.

6.1 RDS 60 activity on proliferation

First, we evaluated this new molecule action on cancer cell viability in two human tumor cell lines, tongue HNSCC CAL 27 and pharynx HNSCC FaDu.

FaDu and CAL 27 cell lines were treated for 24 and 48 h with 100 nM, 1 µM, 2.5 µM, 5 µM, and 10 µM RDS 60.

The first significative reduction of cell survival was seen at 24 h with 2.5 µM RDS 60 on CAL 27 and with 10 µM on FaDu; however, after 48 h of treatment, the proliferation inhibition was significant with 1 µM RDS 60 on both cell lines (Fig. 15).

In a second moment, we wanted to investigate its possible cytotoxicity on normal somatic cells: dermal fibroblasts HF and keratinocytes HaCaT were used.

The two cell lines were treated for 24 and 48 h with 100 nM, 1 µM, 2.5 µM and 10 µM RDS 60.

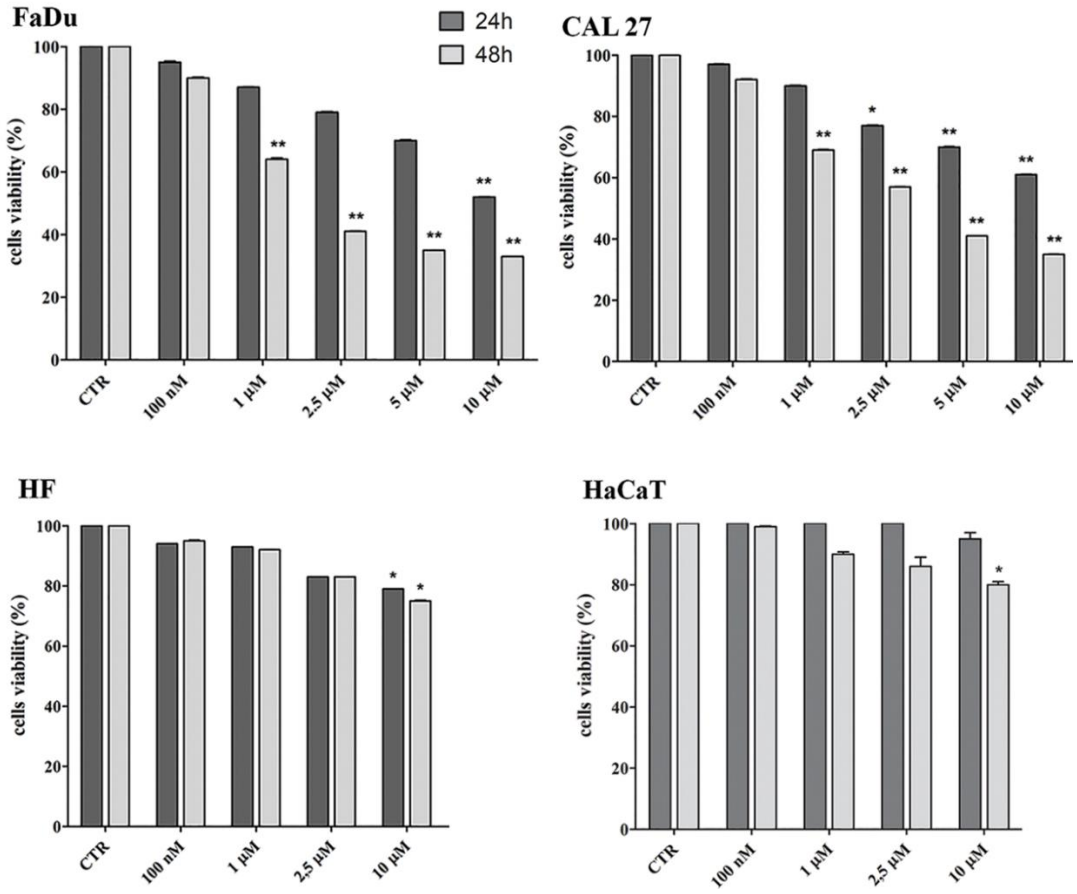

Figure 15: Cell viability of untreated (CTR) and RDS 60 treated FaDu, CAL 27, HF and HaCaT expressed as percentages of alive cells ± SD. Treatments were performed for 24 and 48 h. * $p < 0.01$; ** $p < 0.001$.

As is visible in the figure 15, RDS 60 statistically inhibits proliferation of both somatic cell lines only at the highest concentration (10 µm). For this reason, during succeeding experiments, we treated tumor cell lines with 1 to 2 µm concentrations which were found to be non-cytotoxic on HF and HaCaT.

We repeated the experiments at 24 h and 48 h with different RDS 60 concentrations (1, 10, 20, 30, and 40 µM) to compute the resulted EC50:

- At 24 h 10.8 µM for CAL 27 and 12.4 µM for FaDu.
- At 48 h 2.5 µM for CAL 27 and 2.9 µM for FaDu.

6.2 RDS 60 action on the mitotic spindle assembly

RDS 60 is structurally correlated with nocodazole, a molecule demonstrated to act avoiding normal microtubule organization by binding tubulin subunits; we decided to evaluate RDS 60 activity on mitotic spindle assembly.

For this aim, immunofluorescent staining of beta-tubulin in both HNSCC cell lines was performed and was possible to examine the undergoing mitosis cells. HNSCC cell lines were treated with 1 µM RDS 60 for 24 h.

Data (Fig. 16) show that all untreated cells presented a normal typical bipolar mitotic spindle, contrary to RDS 60 treated cells. In this case, we could see a mitotic spindle characterised by altered shape and size with the tripolar or multipolar organization, defined a starting point to abortive mitosis.

Then we counted mitotic spindles per field and related them to the total cell number quantifying the mitotic index that, as expected, is not significantly modified by RDS 60 treatment:

- 7% in untreated FaDu.
- 5% in treated FaDu.
- 5% in untreated CAL 27.
- 4% in treated CAL 27.

We then performed tubulin immunofluorescence on HF cell line to verify its no-cytotoxic effect. Indeed, we could observe that untreated and 1 µM RDS 60 treated fibroblasts had all normal mitotic spindles.

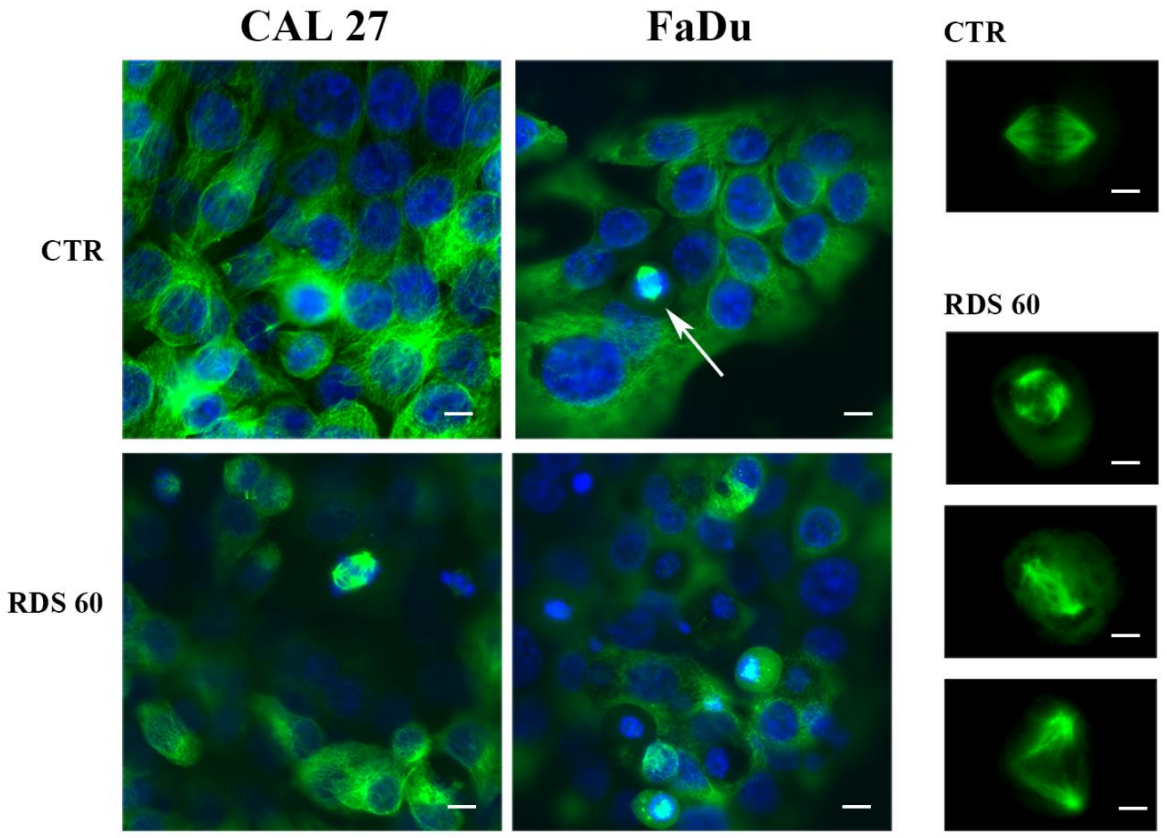

Figure 16: Immunofluorescence staining of beta-tubulin on CAL 27 and FaDu untreated (CTR) and 1 μM RDS 60 treated for 24 h; bar 5 μm. The arrow shows a normal mitotic spindle. Smaller panels show mitotic spindles at higher magnification from untreated (CTR) and RDS 60 treated cells: bar 2 μm.

6.3 RDS 60 induces a cell cycle block in G2/M phase in HNSCC cell lines

We decided to examine RDS 60 as a potential cell cycle checkpoint controller. For this study, we treated HNSCC cell lines (FaDu and CAL 27) with 1 μM RDS 60 for 24 h and then analysed both lines, untreated and RDS 60 treated, by flow cytometry assay. From this experiment result a significant increment of cells in the G2/M step and a corresponding decrement of cells in the S and G0/G1 steps. In terms of percentage, RDS 60 determinates a cell enhancement in the G2/M phase from 27% in untreated to 69% in treated FaDu and from 32% in untreated to 56% in treated CAL 27. (Fig.17)

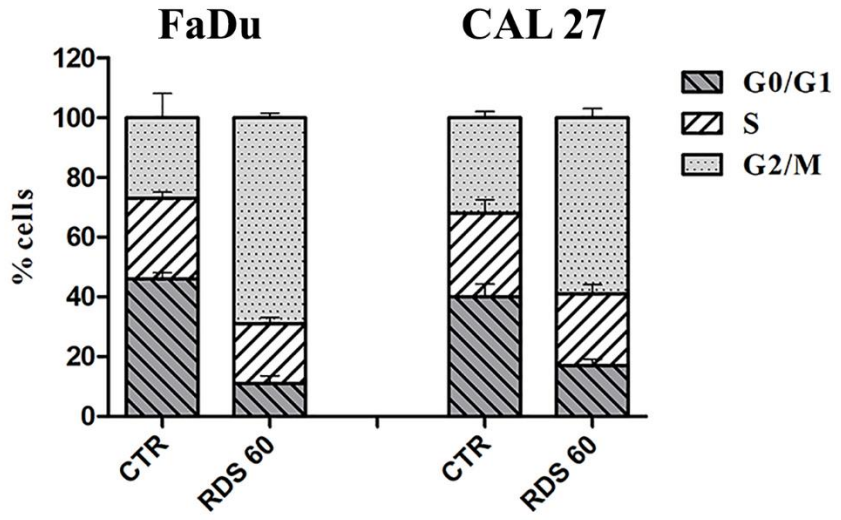

Figure 17: Cell cycle was evaluated by flow cytometry of FaDu and CAL 27 untreated (CTR) and 1 µM RDS 60 treated for 24 h. The histogram shows the media ± SD representative of results obtained from three independent experiments.

6.4 RDS 60 up-regulates cytoplasmatic cyclin B1

RDS 60 induce a significative increment of cytoplasmic cyclin B1 in HNSCC cell lines. Having established that up-regulated cyclin B1 is crucial during regular monitoring of cell cycle transition from S to G2 and then to the M phase [123] we estimated cyclin B1 expression by western blot and by immunofluorescence analysis in cell lines untreated and treated for 24 h with 1 µM RDS 60.

Cyclin B1 was up-regulated in both HNSCC cell lines (Fig. 18) and its immunofluorescent staining was significantly enhanced (Fig. 19). Furthermore, we found that its localization was entirely cytoplasmic (Fig. 19), which means it did not translocate into the nucleus and this result is in harmony with the cell increased block in the G2/M phase, because physiologically cyclin B1 must translocate from cytoplasm into the nucleus to be activated and move the cell cycle from G2 to M phase [123].

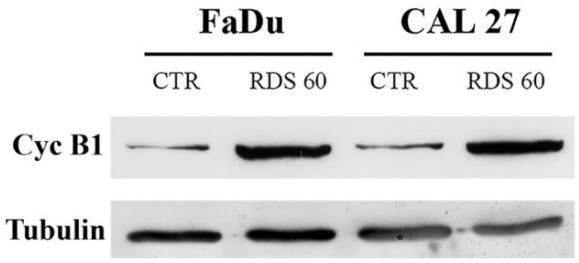

Figure 18: Western blot of cyclin B1 from FaDu and CAL 27 untreated (CTR) and 1 µM RDS 60 treated for 24 h.

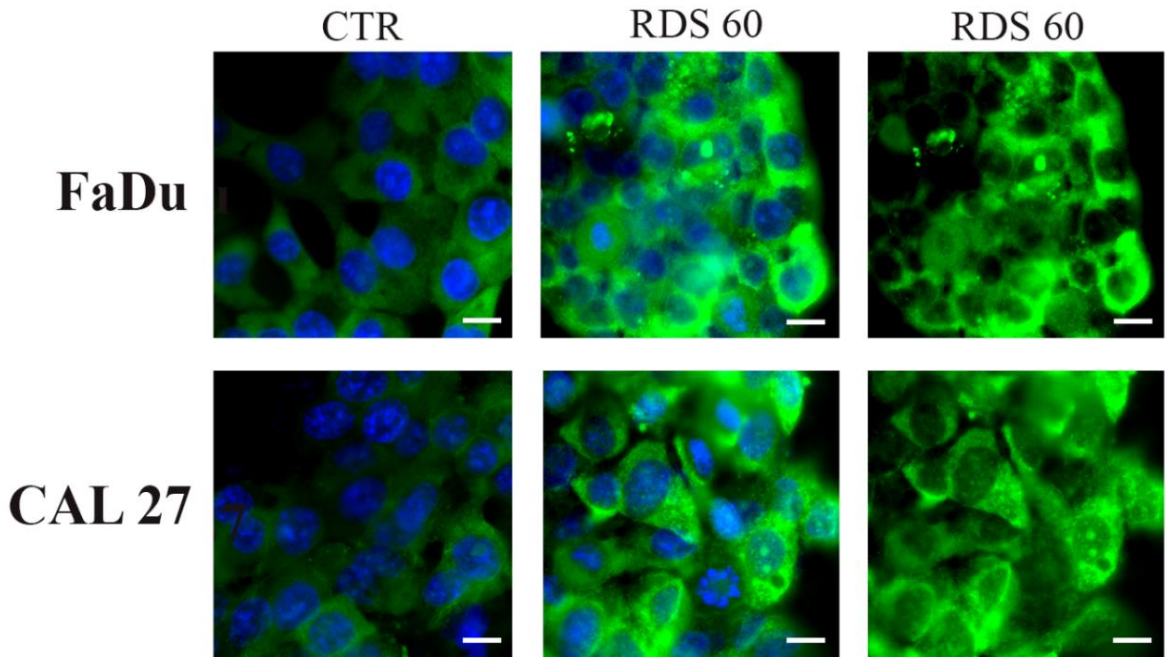

Figure 19: Up-regulation of cytoplasmic cyclin B1 in HNSCC cell lines induced by RDS 60. Immunofluorescence staining of cyclin B1 on FaDu and CAL 27 untreated (CTR) and 1 µM RDS 60 treated for 24 h shown with and without nuclear staining; bar 7 µm.

6.5 RDS 60 leads to apoptotic death in HNSCC cell lines

Cell cycle arrest is an origin point to the apoptosis process, consequently, also RDS 60 role during apoptosis was assessed.

FaDu and CAL 27 were treated with 2 µM RDS 60 for 24 h, then the expression of some proteins involved in that process was analysed by western blot experiments:

- PARP-1, a marker of apoptosis.
- Bax, a pro-apoptotic protein.
- BCL-2, an anti-apoptotic protein.
- Cleaved caspase 8, a marker of apoptosis extrinsic pathway.
- Caspase 9, a marker of apoptosis intrinsic pathway.

We found, as represented below (Fig. 20):

- A reduction of full-length PARP-1, which means apoptosis activation in both HNSCC lines when treated since its cleavage by caspase 3 is observed during apoptosis last phases.
- Up-regulation of Bax and down-regulation of Bcl-2 in treated cells, resulting in an increased Bax/Bcl-2 ratio that is indicative of apoptosis. Bax/Bcl2 ratio was determined by measuring densitometric values of Bax and Bcl2 bands normalized on respective tubulin bands and then calculated by dividing the first value by the second one.
- Proteolytic fragments of caspase 8 and unaltered caspase 9 bands in both cell lines after RDS 60 treatment. This data validates the apoptotic hypothesis because caspase 8 fragments are indicative of its activation; furthermore, it demonstrates the extrinsic pathway activation induced by RDS 60. Additionally, the no-altered caspase 9 expression allows us to exclude that apoptosis is driven by the intrinsic way.

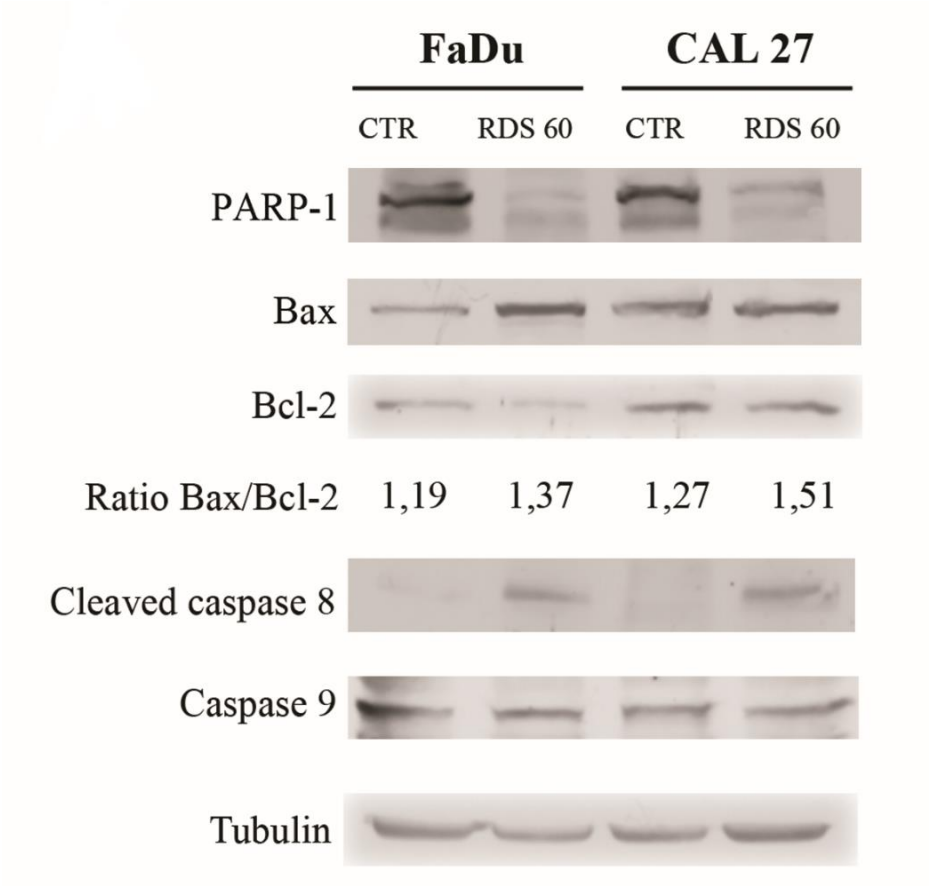

Figure 20: Western blot of PARP-1, Bax, Bcl-2, cleaved caspase 8 and caspase 9 from FaDu and CAL 27 untreated (CTR) and 2 µM RDS 60 treated for 24 h. The values from densitometry quantifications of three different experiments of the Bax to Bcl-2 ratio normalized to tubulin are indicated.

Successively we evaluated apoptosis and necrosis rates to measure tumor cell death induced by RDS 60 treatment.

We treated both HNSCC cell lines with 2 µM RDS 60 for 24 h, then we double-stained cells with APC conjugated annexin V (indicative of apoptosis) and 7AAD and analysed them by flow cytometry.

Data showed a significant Annexin V staining increase after RDS 60 treatment, from 3% to 26% in FaDu and from 5% to 39% in CAL 27 (Fig. 21). On the other hand, the necrosis rate did not significantly change between untreated and treated cells.

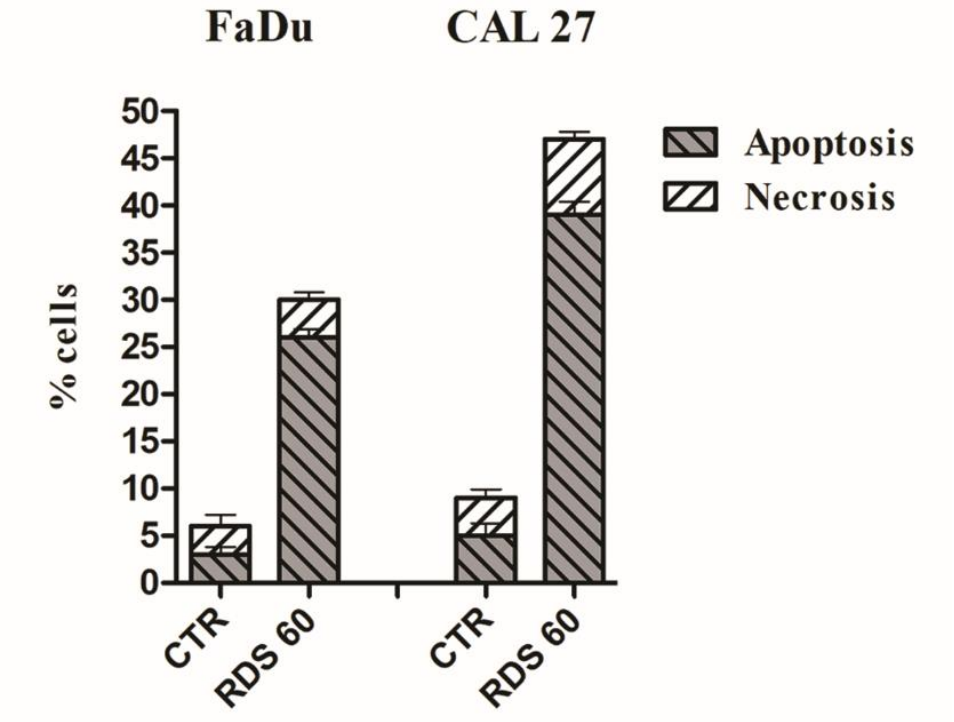

Figure 21: Percentages of apoptotic and necrotic cells evaluated by annexin V-APC and 7AAD expression quantified by FACS on FaDu and CAL 27 untreated (CTR) and 2 μM RDS 60 treated for 24 h. The histogram shows the media ± SD representative of results obtained from two independent experiments.

6.6 RDS 60 implication in EMT regulation and cell migration

To evaluate RDS 60 role in the epithelial-mesenchymal transition (EMT), we analysed the expression of two EMT important markers, E-cadherin and N-cadherin on basal forms and after 24 h with RDS 60 treatment in both HNSCC cell lines.

During the epithelial-mesenchymal transition in malignant cells, E-cadherin normally declines while N-cadherin expression increases.

We used western blotting analysis and discovered that E-cadherin with low basal expression increased after treatment, while N-cadherin, extremely expressed in both untreated cell lines, decreased practically almost to zero in RDS 60 treated cells.

To sum up we can conclude that RDS 60 can reverse the EMT phenotype in FaDu and CAL 27 cell lines.

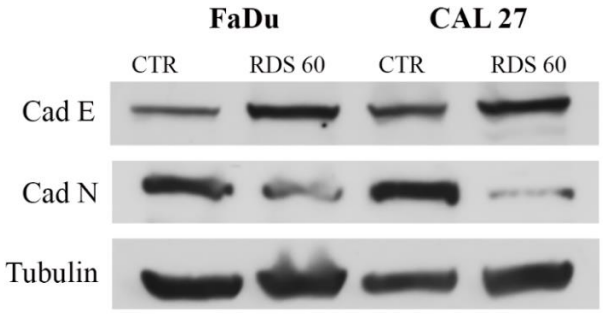

Figure 22: Western blot of EMT related proteins E-cadherin and N-cadherin from untreated (CTR) and 1 μM RDS 60 treated for 24 h FaDu and CAL 27.

In the end we demonstrated that RDS 60 can reduce the invasive phenotype of HNSCC cells.

To this aim, we performed a Matrigel invasion assay on untreated cells and 1 μM RDS 60/16 h treated cells.

Counting the cells able to transfer through the Matrigel we revealed that: (Fig. 23)

- Migrating FaDu cells decreased from 71 to 17, determining the invasion activity inhibition by 76%.
- Migrating CAL 27 reduced from 92 to 23, resulting in a diminishing cell number able to cross over the Matrigel by 75%.

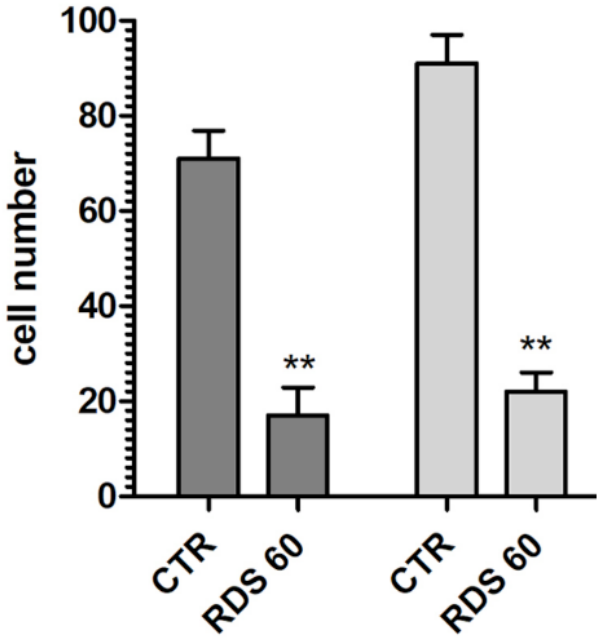

Figure 23: Graphic representing the number of migrated cells in five random fields from three independent experiments of Matrigel invasion assay with the means ± SD; ** $p < 0$.

The microscopy images of the Matrigel invasion assay confirmed a different migrated cell density (Fig. 24):

- High density in untreated HNSCC cell lines.
- Low density in 1 µM RDS 60/ 16 h treated FaDu and CAL 27 lines.

Furthermore, untreated FaDu were characterized by two EMT hallmarks: heterogeneous morphology and mesenchymal phenotype. As can be seen by the high magnification insert.

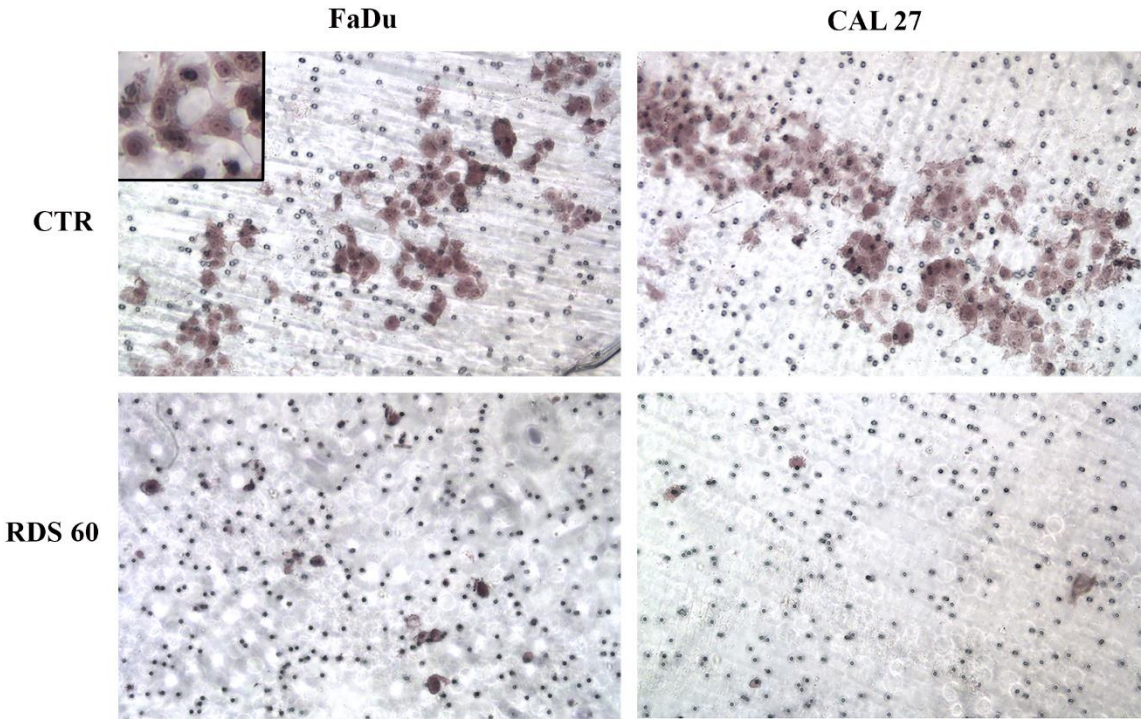

Figure 24: Matrigel invasion assay of untreated FaDu and CAL 27 cells (CTR) and 1 µM RDS 60 treated cells for 16 h. The higher magnification insert on the top left angle shows morphological heterogeneity and mesenchymal phenotype of untreated FaDu.

7. Discussion 2° report

Microtubules are the cytoskeleton base components in eukaryotic cells. The cytoskeleton is a radial network undergoing continuous reorganization cycles during cell division to form a mitotic spindle [68]. Indeed, microtubules play a crucial role during chromosome segregation, but also in cellular vesicle transportation and cell invasion [69].

Microtubules are an interesting therapeutic target, and several researchers are focusing on new anti-microtubular agent development to increase selectivity towards tumor cells and, at the same time, reduce the side effects manifested by many compounds currently in use [124][125]. The success of microtubule-targeting agents used in cancer therapy is limited by side effects including haematological and neurological toxicities and by drug resistance development [126].
Whereby our group synthesized a new compound, named RDS 60, starting from nocodazole, a microtubule targeting compound which, acting on cell cycle, causes mitotic arrest and apoptosis cell death. We wanted to demonstrate this compound to have not undesirable effects on normal cells but, on the other hand, be able to inhibit cancer cells proliferation and other aspects that make cancer a malignant disease.

We chose particularly two cancer lines from head and neck squamous cell carcinomas that need new therapeutic approaches.

Human head and neck squamous cell carcinomas are extremely aggressive tumors with an incidence in continuous growth, representing the sixth leading cause of cancer in the world [2][4].

To sum up, our data reported as following:

1. The effect of RDS 60 on proliferation becomes significant at 48 h with 1 μm RDS 60 in both cancer lines, while at 24 h of treatment the effect turns into significative value with higher concentrations. The compound highlights cytotoxicity on not processed somatic cells, HF and HaCat, only at the highest concentration. Using RDS 60 at lower efficacy concentrations, it will not have any side effects on normal cells.

2. All RDS 60 treated cells reported mitotic spindle characterised by abnormal shape and size with tripolar or multipolar structure inducing the abortive mitosis. We can conclude that RDS 60 takes place on the mitotic spindle assembly.

3. The cell cycle passages are altered, resulting in an increment of cells in the G2/M phase and a decrement of cells in the S and G0/G1 steps. Usually, a cell undergoing a sustained arrest in pro-metaphase gets going to apoptosis [86].

4. RDS 60 up-regulates a crucial cytoplasmatic cell cycle regulator, cyclin B1, and blocked its translocation into the nucleus, avoiding cells to move from G2 to M phase.

5. RDS 60 induce apoptosis activation via extrinsic pathway demonstrated by reduction of full-length PARP-1, caspase 8 cleavage, Bax up-regulation and Bcl-2 down-regulation, resulting in an increased Bax/Bcl-2 ratio, in treated cells. Treated cells evaluated by annexin V-APC and 7AAD expression quantified by FACS reported an unmodified necrosis rate but an increased apoptosis rate.

6. RDS 60 can reverse the EMT phenotype in FaDu and CAL 27 cell lines as suggest the effect on EMT related proteins, E-cadherin and N-cadherin, and the migrated cell count in Matrigel assay. Defined that transition to a mesenchymal-like phenotype provides the migratory and invasive skills to cancer cells [127], RDS 60 decreases tumor motility and infiltration.

To sum up, all these data suggest RDS 60 as a potential innovative anti-tumor compound for head and neck squamous cell carcinomas since it can inhibit cancer cell proliferation, induce apoptosis and reduce cancer invasion. These represent the main malignant tumor features, thus is possible to suppose a cancer regression induced by this compound. With this study, we have place foundations for a further deepening about RDS 60 activity and its hopeful role in cancer therapy.

8.Results 3° report

The kinesin Eg5 inhibitor K858 exerts antiproliferative and proapoptotic effects and attenuates the invasive potential in head and neck squamous carcinoma cells.

Nicolai A; Taurone S; Carradori S; Artico M; Greco A; Scarpa S.

2022, submitted to Investigational New Drugs.

Head and neck squamous cell carcinomas (HNSCC) are a group of aggressive tumors characterized by poor prognosis mainly due to distant metastases [2], multiple primary tumors and inoperable relapses development [107][108].

Therefore, it is necessary to find new therapeutic approaches: it is possible to target kinesin Eg5, whose high expression detected in laryngeal squamous cell carcinoma has been correlated with prognostic grade [100]. Eg5 inhibition leading to mitosis arrest could be a good anti-cancer approach [91].

Furthermore, their lacking interference with the microtubular organization makes them safer than other anti-microtubule agents since, contrary to them, they don't produce neuropathy in patients [91] [128].

A small Eg5 inhibitor, named K858 has been synthesized and found to have significant anti-neoplastic activity in different tumors, including prostate and breast carcinomas, melanoma and glioblastoma [114][115][116][117][118].

In this study, we wanted to demonstrate that K858 antitumor activity can be extended to head and neck squamous cell carcinomas.

8.1 K858 activity on proliferation

In this report we utilized three HNSCC cell lines:

- FaDu, pharynx squamous cell carcinoma.
- CAL 27, tongue squamous cell carcinoma.
- SCC-15, tongue squamous cell carcinoma.

All cell lines were treated for 24 and 48 h with 1 μM, 5 μM, 10 μM K858 and then analysed by the proliferation assay to calculate K858 activity on cell viability and replication.

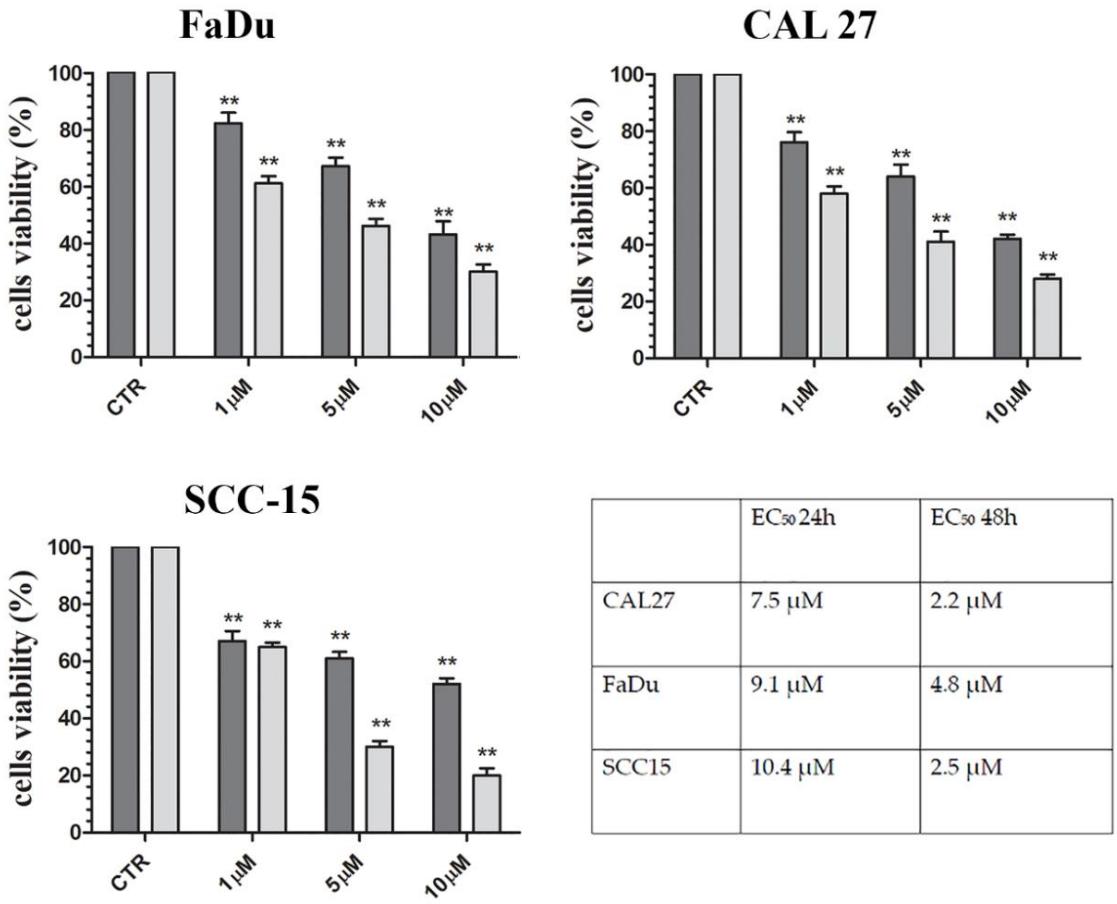

	EC_{50} 24h	EC_{50} 48h
CAL27	7.5 μM	2.2 μM
FaDu	9.1 μM	4.8 μM
SCC15	10.4 μM	2.5 μM

Figure 25: Cell viability of untreated (CTR) and K858 treated FaDu, CAL 27 and SSC-15 cells expressed as percentages of alive cells ±SD. Treatments were performed for 24 h (dark grey) and 48 h (light grey). * p <0.01; ** p <0.001. The table on the right shows EC_{50} values at 24 and 48 h.

A significant proliferation inhibition is detected already at 1 μM K858/ 24h treatment in all three HNSCC lines and continues with a constant reduction directly proportional to the concentration and treatment time increment.

In a second moment, to calculate EC_{50}, each cell line was treated with 1, 10, 20, 30, 40 μM K858 for 24 and 48 h and resulting EC_{50}s are reported in the table (Fig.25).

8.2 K858 action on mitotic spindle assembly

K858 targets specifically kinesin Eg5 so we decided to evaluate the effect of K858 on the tubulin organization. Mitotic kinesin is responsible for mitotic spindle assembly and for this reason we performed the immunofluorescent staining of beta-tubulin in all three

HNSCC cell lines untreated and treated with 1 μM K858 for 24 h and then focused, using a fluorescence microscope, on the undergoing mitosis cells.

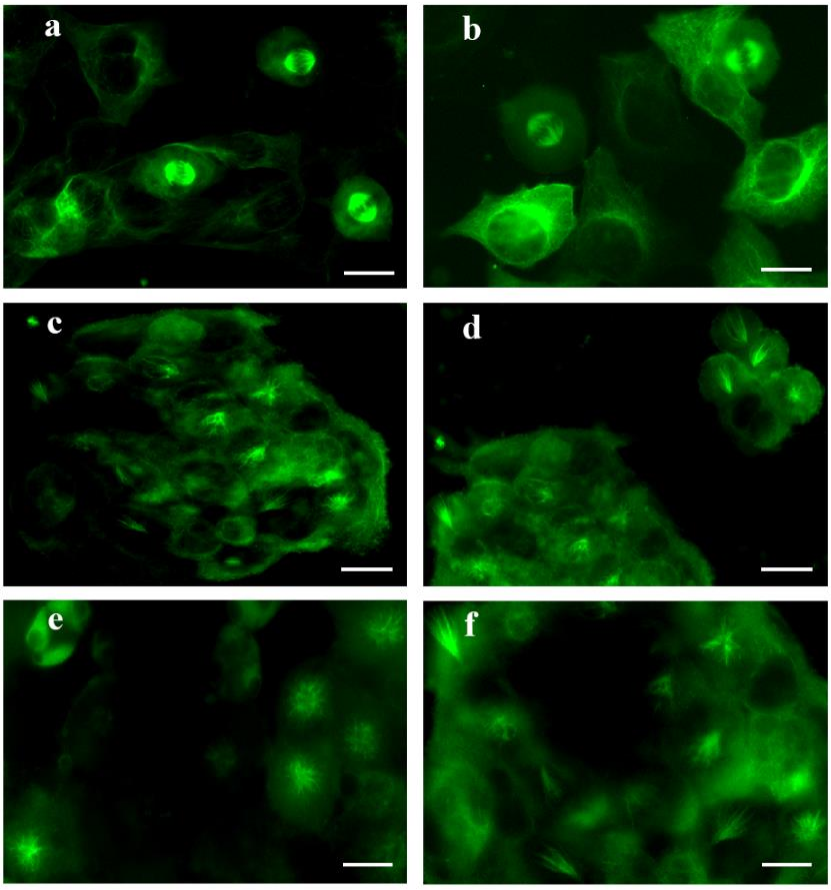

Figure 26: Immunofluorescence staining of beta-tubulin on untreated CAL 27 (a) and untreated FaDu (b) and on CAL 27 (c), FaDu (d) and SCC-15 (e-f) treated with 1 μM K858 for 24 h; bar a: 7 μm, b: 5 μm, c-d: 8 μm, e-f: 7 μm.

As evident by microscope images, it is possible to deduce an alteration of all mitotic spindle forms after K858 treatment:

- Untreated FaDu, CAL 27 and SCC-15 cells had every normal bipolar shaped mitotic spindle (Fig. 26, a-b).
- Treated FaDu, CAL 27 and SCC-15 cells showed every mitotic spindle with abnormal monopolar shapes (Fig. 26, c-f).

8.3 K858 induces a cell cycle block in G2/M phase in HNSCC cell lines

Eg5 inhibition leads to mitosis arrest [91], and after demonstrating the real K858 implication in impairment of mitotic spindle assembly, we evaluated its activity on cell cycle control by flow cytometry.

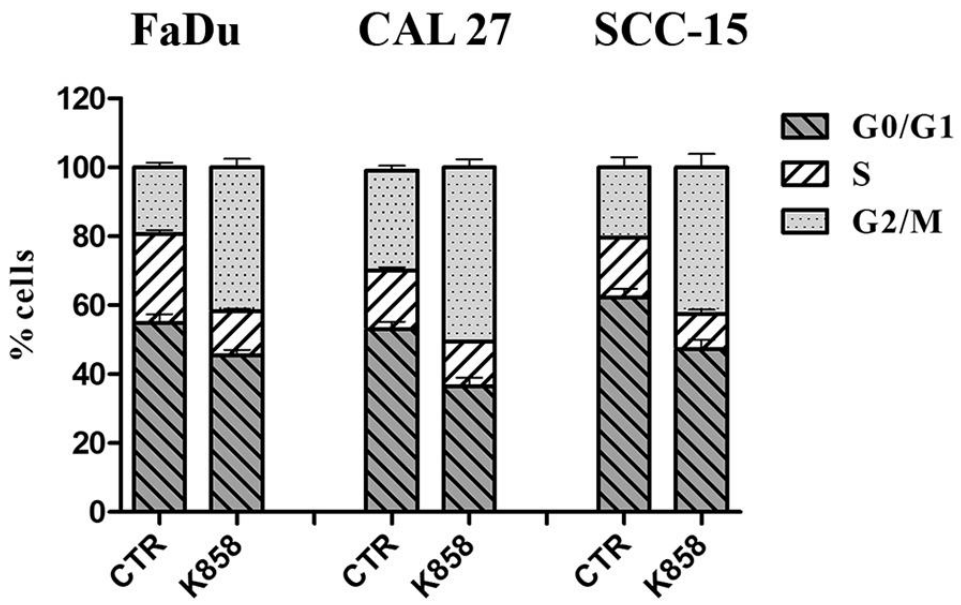

Figure 27: Cell cycle by flow cytometry analysis of FaDu, CAL 27 and SCC-15 cells untreated (CTR) and treated with 1 μM K858 for 24 h. The histogram shows the means ±SD representative of results obtained from three independent experiments.

After 1 μM K858 for 24 h treatment: (Fig. 27)

- FaDu in G2/M phase cells raised from 19.4% to 42%.
- CAL 27 cells from 29.1% to 50.4%.
- SCC-15 cells from 20.3% to 42.4%.

To sum up, K858 treatment induced an increment of cells in the G2/M phase and a corresponding reduction of cells in the S and G0/G1 phases.

8.4 K858 up-regulates cytoplasmatic cyclin B1

Cyclin B1 increased expression is crucial for a normal control in the cell cycle, especially in S/ G2 and G2/M transitions [123].

Each cell line was treated with 1 μM K858 treatment for 24 h and consequently, western blot has been performed. As expected, cyclin B1 was up-regulated in every HNSCC (Fig. 28)

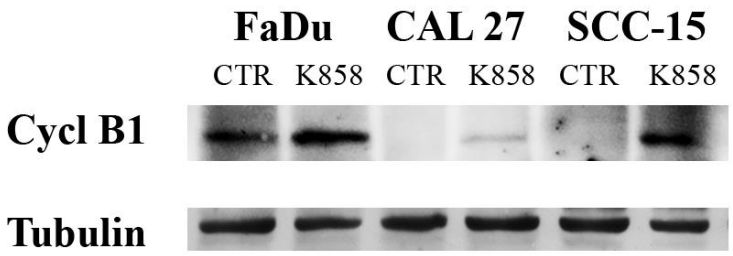

Figure 28: Western blot of cyclin B1 and tubulin in the 3 HNSCC cell lines untreated (CTR) and treated with 1 μM K858 for 24 h.

Cyclin B1 was then analysed by immunofluorescence, confirming that 1 μM K858 treatment for 24 h determined an increase of staining in all three HNSCC; cyclin B1 localization was exclusively cytoplasmic, with no translocation into the nucleus, as shown for SCC-15 cells (Fig. 29).

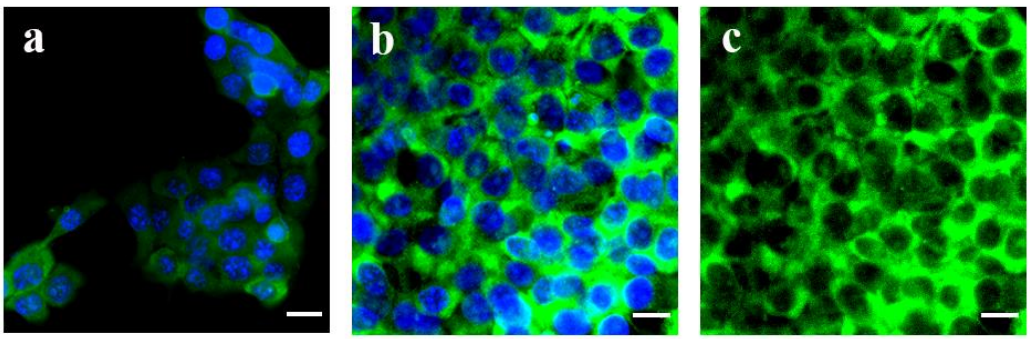

Figure 29: Immunofluorescence staining of cyclin B1 on untreated (a) and treated with 1 μM K858 for 24 h SCC-15 shown with (b) and without (c) nuclear staining; bar 7 μm.

8.5 K858 leads to apoptotic death in HNSCC cell lines

These two last results are suggesting a possible K858 implication on apoptosis induction. Therefore, the following proteins were analysed by western blotting assay after 24 h of 2.5 μM K858 treatment in all three cell lines: (Fig. 30)

- PARP-1, a marker of apoptosis, was cleaved in all three HNSCC.
- Bax, a pro-apoptotic protein, was up-regulated in all cell lines.
- BCL-2, an anti-apoptotic protein, was roughly down-regulated in every cell line.
- Caspase 8, a marker of extrinsic pathway apoptosis, resulted to be cleaved in every cell line after treatment.
- Caspase 9, a marker of intrinsic pathway apoptosis, has been found to decrease only in the SSC-15 cell line.

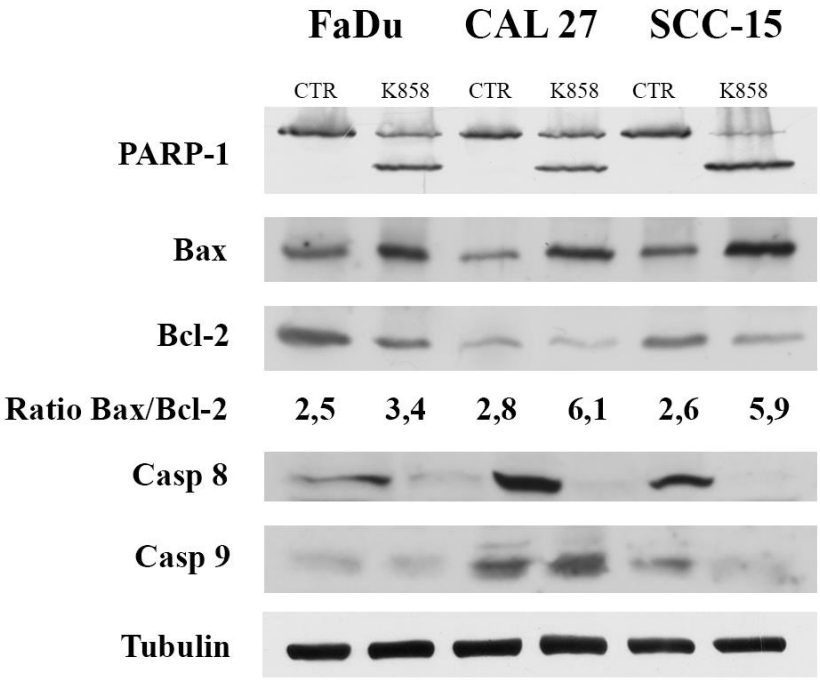

Figure 30: Western blot of PARP-1, Bax, Bcl-2, caspase 8, caspase 9 and tubulin from untreated (CTR) and treated with 2.5 μM K858 for 24 h FaDu, CAL 27 and SCC-15 cells. The means from densitometry quantifications of three different experiments of the Bax to Bcl-2 ratio normalized to tubulin are indicated.

Consequently, it can be concluded that K858 induces apoptosis through the extrinsic pathway in HNSCC cell lines employed because:

- PARP-1 cleavage by caspase 3 appears during the apoptosis late phases.
- Increased Bax/Bcl-2 ratio is an index of apoptosis (single band densitometry was measured and Bax/Bcl2 ratio calculated and reported in the figure 30).
- Cleavage of caspase 8 is indicative of its activation.

In addition, activation of the caspase 9 cleavage in SCC-15 suggests a dual apoptosis mechanism, both intrinsic and extrinsic ones.

8.6 K858 implication in EMT reversion and cell migration

Invasiveness is a characteristic aspect in malign disease, and it is usually sustained by neo-synthesis of lytic enzymes, such as matrix metalloproteases (MMPs) and epithelial-mesenchymal transition (EMT) [129].

We executed a western blot analysis to examine the expression of E-cadherin and N-cadherin, two important EMT markers and MMP1, MMP2 and MMP9, the matrix metalloproteases mainly associated with HNSCC.

Before and after 24 h of 1 μM K858 treatment proteins expression highlighted as follows (Fig. 31):

- E-cadherin, basally lightly expressed, was increased by K858 in all three HNSCC.
- Untreated HNSCC stated N-cadherin of variable intensity, and it decreased significantly after treatment.
- CAL 27 and SCC-15 expressed high levels of MMP2, but not FaDu which expressed exclusively MMP1.
- MMP2 and MMP1 were radically down-regulated in every HNSCC after treatment.
- Evaluable levels of MMP9 have not been found in any employed cells.

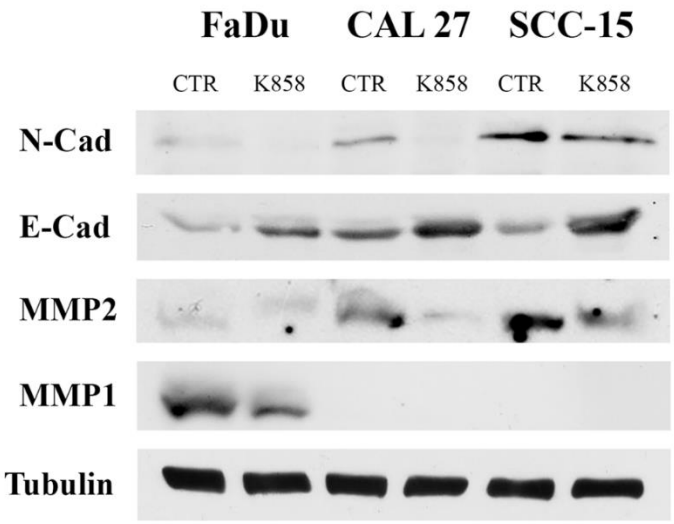

Figure 31: Western blot of N-cadherin, E-cadherin, MMP2, MMP1 and tubulin from untreated (CTR) and 1 μM K858 treated for 24 h FaDu, CAL 27 and SCC-15 cells.

Untreated and treated migrated cells were counted in five different fields showing that K858 reduced invading Fadu by 79%, CAL 27 by 83% and SCC-15 by 73%.

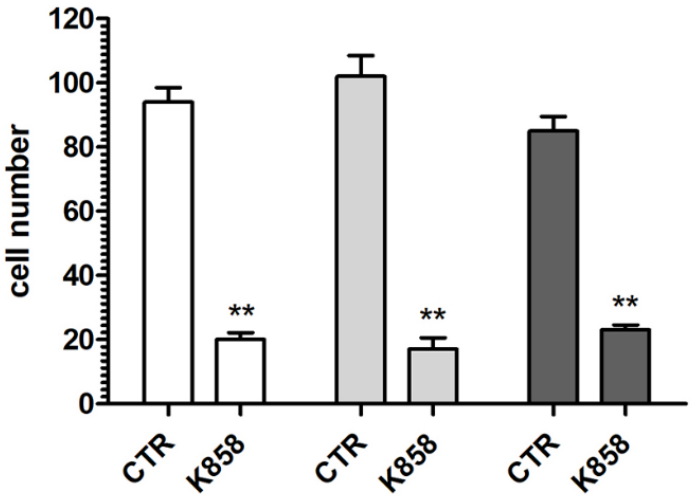

Figure 32: Migrated cells in five random fields from three independent experiments were counted and the means ±SD are reported in the graph with **P<0.001.

In parallel, a Matrigel invasion assay was performed on untreated (CTR) and 16 h/1 μM K858 treated cells: the basal high rate of motility has been drastically reduced after treatment in every HNSCC. (Fig. 33)

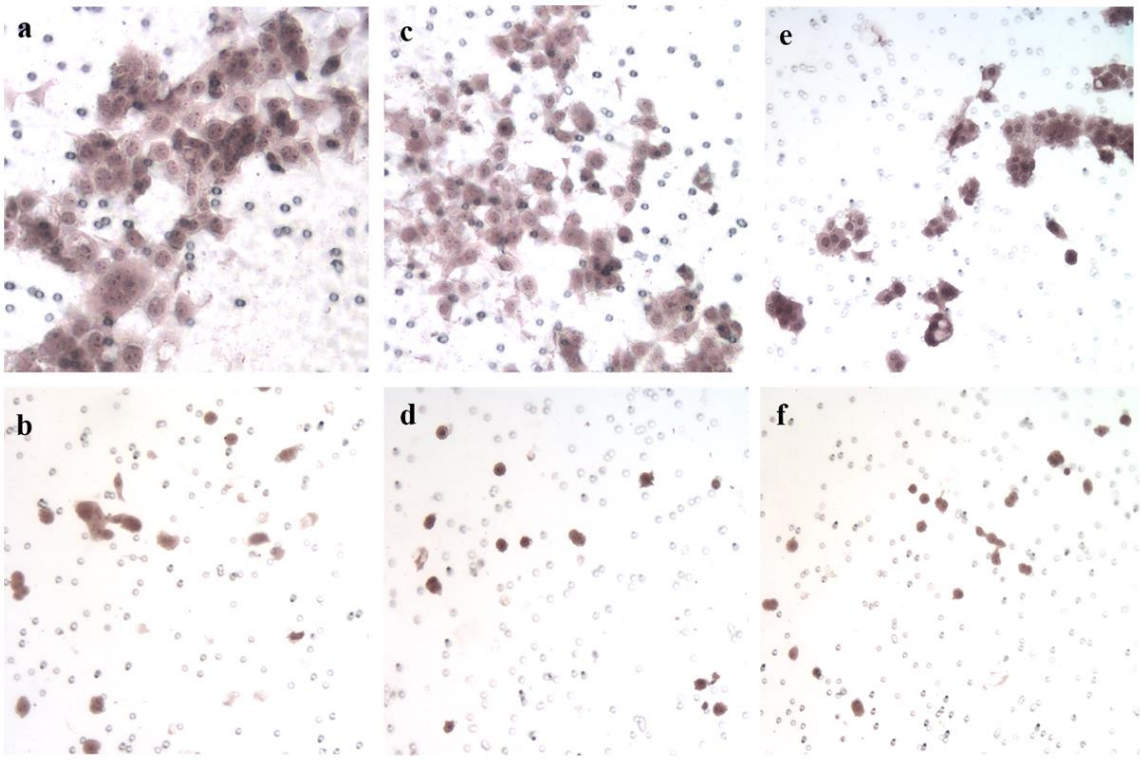

Figure 33: Matrigel invasion assay of FaDu (a-b), CAL 27 (c-d) and SCC-15 (e-f) cells untreated (a, c, e) and treated with 1 μM K858 for 16 h (b, d, f).

9. Discussion 3° report

The cytoskeleton is based on a microtubules network and participates in various cellular activities, including mitosis and transport. Microtubules (MTs) take place in chromosome alignment and segregation [93][94].

Since they are crucial on axonal transport in the central nervous system, the MT targeting compounds are neurotoxic as a side effect [89]. So, our aim was to investigate new MT targeting molecules without these side effects or to block the mitotic process without affecting MT organization.

For this purpose, mitotic kinesins, molecular motors that coordinate different passages in mitotic phase, can be targeted [90]. Eg5, especially, is overexpressed in diverse high proliferative cancers while it is hardly expressed in non-proliferation tissues [96]. Eg5 is involved in the bipolar spindle formation and its inhibition leads to apoptosis in diverse tumor cell lines [97].
Therefore, today some mitotic kinesin inhibitors, developed and utilised in preclinical and clinical studies, have shown not to generate neurotoxicity [91]. Since in the past years our group had defined the K858 anti-tumoral activity, an inhibitor of kinesin Eg5, we decided to evaluate its efficacy on HNSCC cell lines: FaDu, CAL 27 and SCC-15.

Our hopes were high because this compound has already been demonstrated to be active on other tumors, such as prostate and breast carcinomas, melanoma and glioblastoma [115][116][117][118]. Indeed, all reported data evidence that K858 can inhibit proliferation, block cell cycle, induce apoptosis and reduce cell migration and extracellular matrix invasion in all three HNSCC cell lines.

Going into detail:

1. Proliferation inhibition decrement is directly proportional to the increase in concentration and time of treatment, starting from 1 μM K85/24 h.
2. FaDu, CAL 27 and SCC-15 cells revealed all abnormal monopolar featured mitotic spindles after treatment, thus confirming K858 meddling in kinase activity leading to abortive mitosis and consequent apoptosis.
3. The experiments highlighted some apoptosis indices: PARP-1 cleavage, increased Bax/Bcl-2 ratio: Bax is a pro-apoptotic protein, and its up-regulated expression means induced apoptosis as well as the down-regulation of BCL-2, an anti-apoptotic protein. The apoptotic process follows the extrinsic way in all three lines and it is confirmed by caspase

8 activation. In addition, the caspase 9 cleavage in the SCC-15 line demonstrates activation of both pathways.

4. Flow cytometry analysis revealed that the cells blocked in G2/M phase raised up in all three cell lines after treatment.
5. Cyclin B1, a vital regulator for cell cycle transition from S to G2 and then to M phases is up-regulated in every HNSCC ant its localization is exclusively cytoplasmic. When the cell is about to go into the G2 phase the levels of cyclin B1 increase, it is phosphorylated and moves into the nucleus to initiate mitosis [123]. This involves uncontrolled cell growth in these cancer lines. Interestingly, K858 increased cyclin B1, blocked its translocation into the nucleus, impeding to the cell to move from G2 to M phase.
6. K858 induces in all three tumor lines a decrease in N-cadherin and an increase in E-cadherin expressions, reverting EMT. In addition, MMPs are radically down-regulated after K858 treatment, thus it inhibits their activity on creating steps for cellular invasion.
7. As expected, the high rate of basal motility is drastically reduced after K858 treatment as Matrigel invasion assay reported.

Therefore, we can conclude that K858 acts blocking various malignant cancer aspects; in this way this compound has a greater chance to arrest HNSCC progress and induce its regression. Closing, K858 can be an excellent candidate for the development of new therapeutic approaches in human head and neck squamous cell carcinoma treatment.

10. References

1. Ga ´zdzicka J; Golabek K; Strzelczyk JK; Ostrowska Z.
   "Epigenetic modifications in head and neck cancer." Biochem. Genet. 2019, 58, 213–244.
2. Leemans CR; Braakhuis BJ; Brakenhoff RH.
   "The molecular biology of head and neck cancer." Nat. Rev. Canc. 2011, 11, 9–22.
3. Yu AJ; Choi JS; Swanson MS; Kokot NC; Brown TN; Yan G; Sinha UK.
   "Association of race/ethnicity, stage, and survival in oral cavity squamous cell carcinoma: A SEER study." OTO Open 2019, 3.
4. Johnson DE; Burtness B; Leemans CR; Lui VWY; Bauman JE; Grandis JR.
   "Head and neck squamous cell carcinoma." Nat. Rev. Dis. Primers. 2020 ,6, 92.
5. Windon MJ; D'Souza G; Rettig EM; Westra WH; van Zante A; Wang SJ; Ryan WR; Mydlarz WK; Ha PK; Miles BA; Koch W; Gourin C; Eisele DW; Fakhry C.
   "Increasing prevalence of human papillomavirus-positive oropharyngeal cancers among older adults." Cancer 2018, 124(14):2993-2999
6. Fung SY; Lam JW & Chan KC.
   "Clinical utility of circulating Epstein-Barr virus DNA analysis for the management of nasopharyngeal carcinoma." Chin Clin Oncol 2016,5, 18.
7. Osazuwa-Peters N; Simpson MC; Zhao L; Boakye EA; Olomukoro SI; Deshields T; Loux TM; Varvares MA; Schootman M.
   "Suicide risk among cancer survivors: Head and neck versus other cancers." Cancer 2018,124, 4072-4079.
8. Hennessey PT; Westra WH; Califano JA.
   "Human papillomavirus and head and neck squamous cell carcinoma: recent evidence and clinical implications." J Dent Res 2009, 88, 300–306.
9. Tsang CM; Lui VWY; Bruce JP; Pugh TJ; Lo KW.
   "Translational genomics of nasopharyngeal cancer." Semin Cancer Biol 2020, 61, 84–100.
10. Velleuer E; Dietrich R.
    "Fanconi anemia: young patients at high risk for squamous cell carcinoma." Mol Cell Pediatr 2014, 1, 9.
11. Chan KCA; Woo JKS; King A; Zee BCY; Lam WKJ; Chan SL; Chu SWI; Mak C; Tse IOL; Leung SYM; Chan G; Hui EP; Ma BBY; Chiu RWK; Leung SF; van Hasselt AC; Chan ATC; Lo YMD.
    "Analysis of plasma Epstein-Barr virus DNA to screen for nasopharyngeal cancer." N Engl J Med 2014, 377, 513–522.

12. Hecht SS.
"Tobacco smoke carcinogens and lung cancer." J Natl Cancer Inst 1999, 91, 1194–1210.
13. Hoffmann D; Hoffmann I.
"The changing cigarette, 1950–1995." J Toxicol Environ Health 1997,50, 307– 364.
14. Warnakulasuriya S; Straif K.
"Carcinogenicity of smokeless tobacco: Evidence from studies in humans & experimental animals." Indian J Med Res 20218, 148, 681–686.
15. Talamini C R; Bosetti C; La Vecchia C; Dal Maso L; Levi F; Bidoli E; Negri E; C Pasche; Vaccarella S; Barzan L; Franceschi S.
"Combined effect of tobacco and alcohol on laryngeal cancer risk: a case-control study." Cancer Causes Control 2002,13, 957–964.
16. Pai SI; Westra WH.
"Analysis of plasma Epstein-Barr virus DNA to screen for nasopharyngeal cancer." N Engl J Med 2017, 377, 513–522.
17. Brooks PJ; Theruvathu JA.
"DNA adducts from acetaldehyde: implications for alcohol-related carcinogenesis." Alcohol 2005, 35, 187–193.
18. Lee NCJ; Kelly JR; Park HS; An Y; Judson BL; Burtness BA; Husain ZA.
"Patterns of failure in high-metastatic node number human papillomavirus-positive oropharyngeal carcinoma." Oral Oncol 2018, 85, 35–39.
19. Cooper JS; Pajak TF; Forastiere AA; Jacobs J; Campbell BH; Saxman SB; Kish JA; Kim HE; Cmelak AJ; Rotman M; Machtay M; Ensley JF; Chao KSC; Schultz CJ; Lee N; Fu KK.
"Postoperative concurrent radiotherapy and chemotherapy for high-risk squamouscell carcinoma of the head and neck." N Engl J Med 2004, 350, 1937–1944.
20. Bernier J; Domenge C; Ozsahin M; Matuszewska K; Lefèbvre JL; Greiner RH; Giralt J; Maingon P; Rolland F; Bolla M; Cognetti F; Bourhis J; Kirkpatrick A; van Glabbeke M.
"Postoperative irradiation with or without concomitant chemotherapy for locally advanced head and neck cancer." N Engl J Med 2004, 350, 1945–1952.
21. Lee AWM; Law SCK; Foo W; Pooh YF; Cheung FK; Chan DKK; Tung SY; Thaw M; Ho JHC.
"Retrospective analysis of patients with nasopharyngeal carcinoma treated during 1976–1985: survival after local recurrence." Int J Radiat Oncol Biol Phys 1993,26, 773–782.

22. Fakhry C; Zhang Q; Nguyen-Tan PF; Rosenthal D; El-NaggarA; GardenDenis Soulieres AS; Trotti A; Avizonis V; Ridge JA; Harris J; Le QT; Gillison M.
"Human papillomavirus and overall survival after progression of oropharyngeal squamous cell carcinoma." J Clin Oncol 2014, 32, 3365–3373.
23. Syn NL; Teng MWL; Mok TSK; Soo RA.
"De-novo and acquired resistance to immune checkpoint targeting". The Lancet Oncology 2017, 18, e731–e741.
24. Vermorken JB et al.
"Platinum-based chemotherapy plus cetuximab in head and neck cancer." N Engl J Med 2008,359, 1116–1127.
25. Taylor MH; Lee CH; Makker V; Rasco D; Dutcus CE; Wu J; Stepan DE; Shumaker RC; Motzer RJ.
"Phase IB/II trial of Lenvatinib plus pembrolizumab in patients with advanced renal cell carcinoma, endometrial cancer, and other selected advanced solid tumors." J Clin Oncol 2020, 38, 1154–1163.
26. Amit M et al.
"Loss of p53 drives neuron reprogramming in head and neck cancer." Nature 2020;578, 449–454.
27. Canning M; Guo G; Yu M; Myint C; Groves MW; Byrd JK; Cui Y. "Heterogeneity of the head and neck squamous cell carcinoma immune landscape and its impact on immunotherapy." Front Cell Dev Biol 2019,7,52.
28. Peltanova B; Raudenska M; Masarik M.
"Effect of tumor microenvironment on pathogenesis of the head and neck squamous cell carcinoma: a systematic review." Mol Cancer 2019,18, 63.
29. Mager DL; Haffajee AD; Devlin PM; Norris CM; Posner MR; Goodson JM.
"The salivary microbiota as a diagnostic indicator of oral cancer: a descriptive, non-randomized study of cancer-free and oral squamous cell carcinoma subjects." J Transl Med 2005, 3, 27.
30. Banerjee S; Tian T; Wei Z; Peck KN; Shih N; Chalian AA; O'Malley BW; Weinstein GS; Feldman MD; Alwine J; Robertson ES.
"Microbial signatures associated with oropharyngeal and oral squamous cell carcinomas." Sci Rep 2017,7, 4036.
31. Sørensen BS; Busk M; Olthof N; Speel EJ; Horsman MR; Alsner J; Overgaard J.

"Radiosensitivity and effect of hypoxia in HPV positive head and neck cancer cells." Radiother Oncol 2013,108, 500–505.

32. Brizel DM; Sibley GS; Prosnitz LR; Scher RL; Dewhirst MW.
"Tumor hypoxia adversely affects the prognosis of carcinoma of the head and neck." Int J Radiat Oncol Biol Phys 1997, 38, 285–289.
33. Linge A et al.
"Low cancer stem cell marker expression and low hypoxia identify good prognosis subgroups in HPV (−) HNSCC after postoperative radiochemotherapy: a multicenter study of the DKTK-ROG." Clin Cancer Res 2016,22, 2639–2649.
34. Mandal R; Şenbabaoğlu Y; Desrichard A; Havel JJ; Dalin MG; Riaz N; Lee KW; Ganly I. Hakimi AA; Chan TA; Morris LGT.
"The head and neck cancer immune landscape and its immunotherapeutic implications." JCI Insight 2016,1, e89829.
35. Whiteside TL.
"Immunobiology of head and neck cancer." Cancer Metastasis Rev 2005,24, 95–105.
36. Partlová S; Bouček J; Kloudová K; Lukešová E; Zábrodský M; Grega M; Fučíková J; Truxová I; Tachezy R; Špíšek R; Fialová A.
"Distinct patterns of intratumoral immune cell infiltrates in patients with HPV-associated compared to non-virally induced head and neck squamous cell carcinoma." Oncoimmunology 2015,4, e965570.
37. Luukkaa M; Vihinen P; Kronqvist P; Vahlberg T; Pyrhönen S; KähäriVM; Grénman R.
"Association between high collagenase-3 expression levels and poor prognosis in patients with head and neck cancer." Head Neck 2006,28, 225–234.
38. Virós D; Camacho M; Zarraonandia I; García J; Quer M; Vila L; León X.
"Prognostic role of MMP-9 expression in head and neck carcinoma patients treated with radiotherapy or chemoradiotherapy." Oral Oncol 2013,49, 322–325.
39. Nijkamp MM; Span PN; Hoogsteen IJ; van der Kogel AJ; Kaanders JHAM; Bussink J.
"Expression of E-cadherin and vimentin correlates with metastasis formation in head and neck squamous cell carcinoma patients." Radiother Oncol 2011, 99, 344–348.
40. Swartz JE; Pothen AJ; van Kempen PMW; Inge Stegeman I; Formsma FK; Van Cann EM; Willems SM; Grolman W.
"Poor prognosis in human papillomavirus-positive oropharyngeal squamous cell carcinomas that overexpress hypoxia inducible factor-1alpha." Head Neck 2016, 38, 1338–1346.

41. Yang MH; Wu MZ; Chiou SH; Chen PM; Chang SY; Liu CJ; Teng SC; Wu KJ.
"Direct regulation of TWIST by HIF-1alpha promotes metastasis." Nat Cell Biol 2008, 10, 295–305.
42. Zhang Z; Filho MS; Nor JE.
"The biology of head and neck cancer stem cells." Oral Oncol 2012, 48, 1– 9.
43. Yu SS; Cirillo N.
"The molecular markers of cancer stem cells in head and neck tumors." J Cell Physiol 2020, 235, 65–73.
44. Cancer Genome Atlas N.
"Comprehensive genomic characterization of head and neck squamous cell carcinomas." Nature 2015, 517, 576–582.
45. Lui VW et al.
"Frequent mutation of the PI3K pathway in head and neck cancer defines predictive biomarkers." Cancer Discov 2013,3, 761–769.
46. Stransky N et al.
"The mutational landscape of head and neck squamous cell carcinoma." Science 2011,333, 1157–1160.
47. Foy JP et al.
"New DNA methylation markers and global DNA hypomethylation are associated with oral cancer development." Cancer Prev Res (Phila) 2015,8, 1027–1035.
48. Ha PK; Califano JA.
"Promoter methylation and inactivation of tumor-suppressor genes in oral squamous-cell carcinoma." Lancet Oncol 2006,7, 77–82.
49. Karakasheva TA et al.
"IL-6 mediates cross-talk between tumor cells and activated fibroblasts in the tumor microenvironment." Cancer Res 2018,78, 4957–4970.
50. Tsai MS; Chen WC; Lu CH; Chen MF.
"The prognosis of head and neck squamous cell carcinoma related to immunosuppressive tumor microenvironment regulated by IL-6 signaling." Oral Oncol 2019,91, 47–55.
51. Burtness B et al.
"Pembrolizumab alone or with chemotherapy versus cetuximab with chemotherapy for recurrent or metastatic squamous cell carcinoma of the head and neck (KEYNOTE-048): a randomised, open-label, phase 3 study." Lancet 2019,394, 1915–1928.

52. Grandis JR; Melhem MF; Gooding WE; Day R; Holst VA; Wagener MM; Drenning SD; Tweardy DJ.
"Levels of TGF-alpha and EGFR protein in head and neck squamous cell carcinoma and patient survival." J Natl Cancer Inst 1998,90, 824–832.
53. Zhu X; Zhang F; Zhang W; He J; Zhao Y; Chen X.
"Prognostic role of epidermal growth factor receptor in head and neck cancer: a meta-analysis." J Surg Oncol 2013,108, 387–397.
54. Wang Z; Valera JC; Zhao X; Chen Q; Gutkind JS.
"mTOR co-targeting strategies for head and neck cancer therapy." Cancer Metastasis Rev 2017, 36, 491–502.
55. Alamoud KA; Kukuruzinska MA.
"Emerging insights into wnt/beta-catenin signaling in head and neck cancer." J Dent Res 2018, 97, 665–673.
56. Johnson DE; O'Keefe RA; Grandis JR.
"Targeting the IL-6/JAK/STAT3 signalling axis in cancer." Nat Rev Clin Oncol 2018,15, 234–248.
57. Niu MM; Qin JY; Tian CP; Yan XF; Dong FG; Cheng ZQ; Fida G; Yang M; Chen H; Gu YQ.
"Tubulin inhibitors: pharmacophore modeling, virtual screening and molecular docking." Acta Pharmacol Sin. 2014, 35, 967–979.
58. Jordan MA; Wilson L.
"Microtubles and actin flaments: dynamic targets for cancer chemotherapy." Curr Opin Cell Bio. 1998,10,123–30.
59. Matson DR; Stukenberg PT.
"Spindle poisons and cell fate: a tale of two pathways." Mol Interv. 2011,11,141–50.
60. Parker AL; Kavallaris M; McCarroll JA.
"Microtubules and their role in cellular stress in cancer." Front Oncol. 2014, 4:153
61. Arnst KE; Wang Y; Lei ZN; Hwang DJ; Kumar G; Ma D; Parke DN; Chen Q; Yang J, White SW; Seagroves TN; Chen ZS; Miller DD; Li W.
"Colchicine binding site agent DJ95 overcomes drug resistance and exhibits antitumor efficacy." Mol Pharmacol. 2019, 96,73–89.
62. Binarová P; Tuszynski J.
"Tubulin: Structure, Functions and Roles in Disease." Cells 2019, 8, 1294.
63. van Eerden RAG; Mathijssen RHJ; Koolen SLW.

"Recent clinical developments of nanomediated drug delivery systems of taxanes for the treatment of cancer." Int J Nanomedicine. 2020, 15,8151–8166.

64. Wani MC; Taylor HL; Wall ME; Coggon P; McPhail AT.
"Plant antitumor agents. VI. The isolation and structure of taxol, a novel antileukemic and antitumor agent from Taxus brevifolia. J Am Chem Soc. 1971, 93, 2325–2327.
65. Van De Water L; Olmstedg JB.
"The quantitation of tubulin in neuroblastoma cells by radioimmunoassay." J Biol Chem. 1980; 255,10744–51.
66. Loiodice I; Janson ME; Tavormina P; Schaub S; Bhatt D; Cochran R; Czupryna J; Fu C; Tran PT.
"Quantifying tubulin concentration and microtubule number throughout the fission yeast cell cycle." Biomolecules. 2019, 9, e23.
67. Lebok P et al.
"High levels of class III beta-tubulin expression are associated with aggressive tumor features in breast cancer." Oncol. Lett. 2016, 11, 1987–1994.
68. Hevia LG; Fanarraga ML.
"Microtubule cytoskeleton-disrupting activity of MWCNTs: applications in cancer treatment." J Nanobiotechnology 2020,18, 181.
69. Borisy G, Heald R, Howard J, Janke C, Musacchio A, Nogales E.
"Microtubules: 50 years on from the discovery of tubulin." Nat Rev Mol Cell Biol. 2016,9,322–8.
70. Brouhard GJ.
"Dynamic instability 30 years later: complexities in microtubule growth and catastrophe." Mol Biol Cell. 2015,55,1207–10.
71. Mitchison T; Kirschner M.
"Dynamic instability of microtubule growth." Nature. 2016, 312,237–42.
72. Yue XJ; Cui XW; Zhang Z; Hu WF; Li ZF; Zhang YM; Li YZ.
"Effects of transcriptional mode on promoter substitution and tandem engineering for the production of epothilones in Myxococcus xanthus. Appl Microbiol Biotechnol. 2018, 102, 5599–5610.
73. Bajaj M; Srayko M.
"Laulimalide Induces Dose-Dependent Modulation of Microtubule Behaviour in the C. elegans Embryo." PLoS One. 2013, 8, e71889.
74. Lee CT; Huang YW; Yang CH; Huang KS.

"Drug delivery systems and combination therapy by using vinca alkaloids"
Curr Top Med Chem. 2015,15, 1491–1500.

75. Moudi M; Go R; Yien CY; Nazre M.
"Vinca Alkaloids." Int. J. Prev. Med. 2013, 4, 1231–1235.
76. Zhang HY; Tang X; Li HY; Liu XL.
"A lipid microsphere vehicle for vinorelbine: Stability, safety and pharmacokinetics." Int. J. Pharm. 2008, 348, 70–79.
77. Drummond DC; Noble CO; Guo Z; Hayes ME; Park JW; Ou CJ; Tseng YL; Hong K; Kirpotin DB.
"Improved pharmacokinetics and efficacy of a highly stable nanoliposomal vinorelbine." J. Pharmacol. Exp. Ther. 2009, 328, 321–330.
78. Rhomberg W; Wink A; Pokrajac B; Eiter H; Hackl A; Pakisch B; Ginestet A; Lukas P; Potter R.
"Treatment of vascular soft tissue sarcomas with razoxane, vindesine, and radiation." Int. J. Radiat. Oncol. Biol. Phys. 2009, 74,187–191.
79. DiJoseph JF; Dougher MM; Evans DY; Zhou BB; Damle NK.
"Preclinical anti-tumor activity of antibody-targeted chemotherapy with CMC-544 (inotuzumab ozogamicin), a CD22-specific immunoconjugate of calicheamicin, compared with non-targeted combination chemotherapy with CVP or CHOP." Cancer Chemother. Pharmacol. 2011,67,741–749.
80. Shrivastava N; Naim MJ; Alam MJ; Nawaz F; Ahmed S; Alam O.
"Benzimidazole scaffold as anticancer agent: Synthetic approaches and structure-activity relationship." Arch. Pharm. 2017, 350.
81. Messore A et al.
"Novel symmetrical benzazolyl derivatives endowed with potent anti-heparanase activity." J. Med. Chem. 2018, 61, 10834–10859.
82. Florian S; Mitchison TJ.
"Anti-microtubule drugs." Methods Mol. Biol. 2016, 1413, 403–421.
83. Vasquez RJ; Howell B; Yvon AM; Wadsworth P; Cassimeris L.
"Nanomolar concentrations of nocodazole alter microtubule dynamic instability in vivo and in vitro." Mol. Biol. Cell 1997, 8, 973–985.
84. Jordan MA; Thrower D; Wilson L.
"Effects of vinblastine, podophyllotoxin and nocodazole on mitotic spindles. Implications for the role of microtubule dynamics in mitosis. J. Cell Sci. 1992, 102, 401–416.

85. Fraschini R.
"Factors that control mitotic spindle dynamics." Adv. Exp. Med. Biol. 2017, 925, 89–101.
86. Zhou J; Giannakakou P.
"Targeting microtubules for cancer chemotherapy." Curr. Med. Chem. Anticancer Agents 2005, 5, 65–71.
87. Frezzato F; Trimarco V; Martini V; Gattazzo C; Ave E; Visentin A; Cabrelle A; Olivieri V; Zambello R; Facco M; Zonta F; Cristiani A; Brunati AM; Moro S; Semenzato G; Trentin L.
"Leukemic cells from chonic lymphocytic leaukemia patients undergo apoptosis following microtubule depolymerization and Lyn inhibition by nocodazole." Br. J. Haematol. 2014, 165, 659–672.
88. Wang Y; Zhang H; Gigant B; Yu Y; Wu Y; Chen X; Lai Q; Yang Z; Chen Q; Yang J.
"Structure of a diverse set of colchicine binding site inhibitors in complex with tubulin provide a rationale for drug discovery." FEBS J. 2016, 283, 102–111.
89. Canta A; Chiorazzi A; Cavaletti G.
"Tubulin: a target for antineoplastic drugs into the cancer cells but also in the peripheral nervous system." Curr Med Chem. 2009, 16, 1315–1324.
90. Cross RA; Mc Ainsh A.
"Prime movers: the mechanochemistry of mitotic kinesins." Nat Rev Mol Cell Biol. 2014, 15, 257–271.
91. Rath O; Kozielski F.
"Kinesins and cancer." Nat Rev Cancer. 2012, 12, 527–539
92. Wordeman L.
"Cytoskeleton and human disease. in: Kavallaris M." (Ed.) 2012. Chapter 3: The Kinesin Superfamily.
93. Goshima G; Scholey JM.
"Control of mitotic spindle length." Annual Review of Cell and Developmental Biology. 2010, 26, 21–57.
94. Bodrug T et al.
"The kinesin-5 tail domain directly modulates the mechanochemical cycle of the motor domain for anti-parallel microtubule sliding." eLife 2020, 9, e51131.
95. Vale RD; Milligan RA.
"The way things move: looking under the hood of molecular motor proteins." Science 2000, 288, 88-95.

96. Castillo A; Morse HC 3rd; Godfrey VL; Naeem R; Justice MJ.
"Overexpression of Eg5 causes genomic instability and tumor formation in mice." Cancer Res. 2007,67,10138-10147.

97. Nakai R; Iida S; Takahashi T; Tsujita T; Okamoto S; Takada C; Akasaka K; Ichikawa S; Ishida H; Kusaka H; Akinaga S; Murakata C; Honda S; Nitta M; Saya H; Yamashita Y.
"K858, a novel inhibitor of mitotic kinesin Eg5 and antitumor agent, induces cell death in cancer cells." Cancer Res. 2009, 69, 3901-3909.

98. Singh SK; Pandey H; Al-Bassam J; Gheber L.
"Bidirectional motility of kinesin-5 motor proteins: structural determinants, cumulative functions and physiological roles." Cellular and Molecular Life Sciences 2018,75,1757–1771.

99. El-Nassan HB.
"Advances in the discovery kinesin spindle protein (Eg5) inhibitors as antitumor agents." E J Med Chem. 2013, 62, 614-631.

100. Lu M; Zhu H; Wang X; Zhang D; Xiong L; Xu l; You Y.
"The prognostic role of Eg5 expression in laryngeal squamous cell carcinoma." Pathology 2016, 48, 214–218.

101. Sun D; Lu J; Ding K; Bi D; Niu Z; Cao Q; Zhang J; Ding S.
"The expression of Eg5 predicts a poor outcome for patients with renal cell carcinoma." Med Oncol 2013, 30,476.

102. Ding S; Xing N; Lu J; Zhang H; Nishikawa K; Liu S; Yuan X; Qin Y; Liu Y; Ogawa O; Nishiyama H.
"Overexpression of Eg5 predicts unfavorable prognosis in non-muscle invasive bladder urothelial carcinoma." Int J Urol 2011, 18, 432–8.

103. Wissing MD; De Morrée ES; Dezentjé VO; Buijs JT; De Krijger RR; Smit VTHBM, Van Weerden WM; Gelderblom H; van der Pluijm G.
"Nuclear Eg5 (kinesin spindle protein) expression predicts docetaxel response and prostate cancer aggressiveness." Oncotarget 2014, 5, 7357–67.

104. Mayer TU; Kapoor TM; Haggarty SJ; King RW; Schreiber SL; Mitchison TJ.
"Small molecule inhibitor of mitotic spindle bipolarity identified in a phenotype-based screen." Science 1999; 286, 971-974.

105. Maliga Z; Xing J; Cheung H; Juszczak LJ; Friedman JM; Rosenfeld SS.
"A pathway of structural changes produced by monastrol binding to Eg5." J Biol Chem. 2006, 281, 7977-7982.

106. Haque SA; Hasaka TP; Brooks AD; Lobanov PV; Baas PW.
"Monastrol, a prototype anti-cancer drug that inhibits a mitotic kinesin, induces rapid bursts of axonal outgrowth from cultured postmitotic neurons." Cell Motil Cytoskel. 2004, 58,10-16.

107. Zhang WL; Zhu ZL; Huang MC; Tang YJ; Tang YL; Liang XH. "Susceptibility of multiple primary cancers in patients with head and neck cancer: Nature or nurture?" Front. Oncol. 2019, 9, 1275.

108. Tabor MP; Brakenhoff RH; Ruijter-Schippers HJ; van der Wal JE; Snow GB. Leemans CR; Braakhuis BJM.
"Multiple head and neck tumors frequently originate from a single preneoplastic lesion. Am. J. Pathol. 2002, 161, 1051–1060.

109. Di Villeneuve L; Souza IL; Tolentino FDS; Ferrarotto R; Schvartsman G.
"Salivary gland carcinoma: Novel targets to overcome treatment resistance in advanced disease." Front. Oncol. 2020, 10, 580141.

110. Ghafouri-Fard S; Gholipour M; Taheri M; Shirvani Farsani Z.
"MicroRNA profile in the squamous cell carcinoma: Prognostic and diagnostic roles." Heliyon 2020, 6, e05436.

111. Robert BM; Dakshinamoorthy M; Ganapathyagraharam Ramamoorthy B; Dhandapani M; Thangaiyan R; Muthusamy G; Madhavan Nirmal R; Rajendra Prasad N. "Predicting tumor sensitivity to chemotherapeutic drugs in oral squamous cell carcinoma patients." Sci. Rep. 2018, 8, 15545.

112. Da Silva SD; Hier M; mLynarek A; Kowalski LP; Alaoui-Jamali MA.
"Recurrent oral cancer: Current and emerging therapeutic approaches." Front. Pharmacol. 2012, 3, 149.

113. Taglieri L; Saccoliti F; Nicolai A; Peruzzi G; Madia VN; Tudino V; Messore A; Di Santo R; Artico M; Taurone S; Salvati M; Costi R; Scarpa S.
"Discovery of a pyrimidine compound endowed with antitumor activity." Invest. New Drugs 2020, 38, 39–49.

114. Nakai R; Iida S; Takahashi T; Tsujita T; Okamoto S; Takada C; Akasaka K; Ichikawa S; Ishida H; Kusaka H; Akinaga S; Murakata C; Honda S; Nitta M; Saya H; Yamashita Y.
"K858, a novel inhibitor of mitotic kinesin Eg5 and antitumor agent, induces cell death in cancer cells." Cancer Res 2009, 69, 3901-3909

115. De Monte C; Carradori S; Secci D; D'Ascenzio M; Guglielmi P; Mollica A; Morrone S; Scarpa S; Aglianò AM; Giantulli S; Silvestri I.
"Synthesis and pharmacological screening of a large library of 1,3,4-thiadiazolines as innovative therapeutic tools for the treatment of prostate cancer and melanoma." Eur J Med Chem 2015,105:245-262.

116. Giantulli S; De Iuliis F; Taglieri L; Carradori S; Menichelli G; Morrone S; Scarpa S; Silvestri I.
"Growth arrest and apoptosis induced by kinesin Eg5 inhibitor K858 and by its 1,3,4-thiadiazoline analogue in tumor cells." Anticancer Drugs 2018,29, 674-681.

117. De Iuliis F; Taglieri L; Salerno G; Giuffrida A; Milana B; Giantulli S; Carradori S; Silvestri I; Scarpa S.
"The kinesin Eg5 inhibitor K858 induces apoptosis but also surviving-related chemoresistance in breast cancer cells." Invest New Drugs 2016, 34, 399-406.

118. Taglieri L; Rubinacci G; Giuffrida A; Carradori S; Scarpa S.
"The kinesin Eg5 inhibitor K858 induces apoptosis and reverses the malignant phenotype in human glioblastoma cells." Invest New Drugs 2018, 36:28-35.

119. Massa S; Di Santo R; Artico M.
"Potential antitumor agents. IV. Pyrrole analogues of oncodazole." J. Heterocycl. Chem. 1990, 27, 1131–1133.

120. Taglieri L; Nardo T; Vicinanza R; Ross JM; Scarpa S; Coppotelli G.
"Thyroid hormone regulates fibronectin expression through the activation of hypoxia inducible factor 1. Biochem. Biophys. Res. Commun. 2017, 493, 1304–1310.

121. Khattab M; Al-Karmalawy AA.
"Revisiting activity of some nocodazole analogues as potential anticancer drugs using molecular docking and DFT calculations." Front. Chem. 2021.

122. Lu Y; Chen J; Xiao M; Li W; Miller DD.
"An overview of tubulin inhibitors that interact with the colchicine binging site." Pharm. Res. 2012, 29, 2943–2971.

123. Hagting A; Jackman M; Simpson K; Pines J.
"Translocation of cyclin B1 to the nucleus at phophase requires a phosphorylation dependent nuclear import signal." Curr. Biol. 1999, 9, 680–689.

124. Dumontet C; Jordan MA.
"Microtubule-binding agents: A dynamic field of cancer therapeutics." Nat. Rev. Drug Discov. 2010, 9, 790–803.

125. Jordan MA; Wilson L.
"Microtubules as a target for anticancer drugs." Nat. Rev. Cancer 2004, 4, 253–265.
126. Mukhtar E; Adhami VA; Mukhtar H.
"Targeting microtubules by natural agents for cancer therapy." Mol. Cancer Ther. 2014, 13, 275–284.
127. Liarte S; Bernabé-García A.; Nicolás FJ.
"Human skin keratinocytes on sustained TGF-β stimulation reveal partial EMT features and weaken growth arrest responses." Cells 2020, 9, 306
128. Cioroiu C; Weimer LH.
"Update on chemotherapy-induced peripheral neuropathy." Curr Neurol Neurosci Rep 2017, 17:47.
129. Meirson T; Samson HGAO.
"Invasion and metastasis: the elusive hallmark of cancer." Oncogene 2019, 30,2024-2026.